A noncanonical GTPase signaling mechanism controls exit from mitosis in budding yeast.

Xiaoxue Zhou[1, 2, *], Shannon Y. Weng[1], Stephen P. Bell[1], Angelika Amon[1]

[1]Department of Biology, David H. Koch Institute for Integrative Cancer Research, Howard Hughes Medical Institute, Massachusetts Institute of Technology, Cambridge, MA 02139, USA

[2]Department of Biology, New York University, New York, NY 10003, USA

[*]Correspondence to: snow.zhou@nyu.edu

ABSTRACT

In the budding yeast *Saccharomyces cerevisiae*, exit from mitosis is coupled to spindle position to ensure successful genome partitioning between mother and daughter cell. This coupling occurs through a GTPase signaling cascade known as the mitotic exit network (MEN). The MEN senses spindle position via a Ras-like GTPase Tem1 which localizes to the spindle pole bodies (SPBs, yeast equivalent of centrosomes) during anaphase and signals to its effector protein kinase Cdc15. How Tem1 couples the status of spindle position to MEN activation is not fully understood. Here, we show that Cdc15 has a relatively weak preference for $Tem1^{GTP}$ and Tem1's nucleotide state does not change upon MEN activation. Instead, we find that Tem1's nucleotide cycle establishes a localization-based concentration difference in the cell where only $Tem1^{GTP}$ is recruited to the SPB, and spindle position regulates the MEN by controlling Tem1 localization. SPB localization of Tem1 primarily functions to promote Tem1-Cdc15 interaction for MEN activation by increasing the effective concentration of Tem1. Consistent with this model, we demonstrate that artificially tethering Tem1 to the SPB or concentrating Tem1 in the cytoplasm with genetically encoded multimeric nanoparticles could bypass the requirement of $Tem1^{GTP}$ and correct spindle position for MEN activation. This localization/concentration-based GTPase signaling mechanism for Tem1 differs from the canonical Ras-like GTPase signaling paradigm and is likely relevant to other localization-based signaling scenarios.

INTRODUCTION

Small GTPases are key regulators in many cellular processes including cell signaling, actin organization, and membrane trafficking[1]. They typically function as molecular switches whose interaction with downstream effectors are regulated by changing nucleotide state[2]. Their high affinity for guanine nucleotides and low intrinsic GTP hydrolysis and GDP/GTP exchange activities underlie their success as molecular switches. Regulatory proteins such as GTPase activating proteins (GAPs) and guanine nucleotide exchange factors (GEFs) control these switches by modulating their GTP/GDP state in response to specific inputs[3]. A classic example is the founding member of the family, Ras, which regulates cell proliferation in response to growth factors[4]. Binding of growth factors to receptors at the cell surface leads to the recruitment of a GEF to the membrane, which promotes the conversion of membrane anchored Ras^{GDP} to Ras^{GTP}. Ras^{GTP} then recruits and activates downstream effectors to signal proliferation. Although well established, it is unclear whether the same switch mechanism applies to all small GTPases involved in cell signaling.

The mitotic exit network (MEN) is a GTPase signaling cascade in the budding yeast *Saccharomyces cerevisiae* that regulates the exit from mitosis where the mitotic spindle disassembles, the nucleus divides, and chromosomes decondense. In budding cells, the site of cytokinesis or division plane is specified by the bud neck prior to mitosis[5]. To ensure proper genome partitioning, the mitotic spindle must be aligned along the mother-bud axis. The spindle position checkpoint (SPoC) blocks exit from mitosis until a spindle pole successfully enters the bud (Fig. 1A). This checkpoint is executed by establishing two zones in the cell with spatially distributed proteins (an inhibitory zone in the mother compartment and an activating zone in the bud)[6,7] and a sensor, the MEN, which integrates multiple signals including spindle position to regulate cell cycle progression[8] (Fig. 1A-B). Only when a spindle pole escapes the inhibitory zone in the mother and enters the activating zone in the bud in anaphase is the MEN activated, triggering mitotic exit. If the spindle is mis-positioned and remains entirely in the mother cell's inhibitory zone, the MEN is kept inactive, arresting the cell in anaphase. Spindle position is transmitted to the MEN through the small GTPase Tem1[9,10]. How Tem1 senses and couples spindle position to MEN activation is not well understood.

Like Ras, Tem1 undergoes a GTP/GDP nucleotide cycle and Tem1's nucleotide states play an important role in its function. Mutations that block GTP hydrolysis and lock Tem1 in the

51 GTP state are constitutively active and bypass the SPoC[11]. Conversely, nucleotide binding
52 mutants that bias Tem1 toward the GDP state render the protein inactive and arrest cells in
53 anaphase even with a correctly positioned spindle[12]. Given these findings, it has been assumed
54 that Tem1 functions as a molecular switch like Ras and spindle position regulates Tem1 by
55 changing its nucleotide state (Fig. 1C).
56 However, there are several aspects of Tem1 biology that are unusual for a small GTPase.
57 First, while the GTP hydrolysis rate of Tem1 is accelerated by a bipartite GAP complex Bub2-
58 Bfa1[10,13], Tem1 does not appear to require a GEF to function, likely due to a relatively fast
59 intrinsic nucleotide exchange rate[13]. As a result, the only way to regulate Tem1's nucleotide state
60 is by modulating the activity of the GAP. The polo-like kinase Cdc5 phosphorylates Bfa1[14]
61 which was shown to reduce Bub2-Bfa1 GAP activity in vitro[15]. Thus, a prevailing model is that
62 the MEN is activated by inactivating the GAP[14–17]. A second peculiar aspect of Tem1 is that its
63 cellular localization correlates with MEN activity[10,18,19] (Fig. 1A). When the spindle is correctly
64 positioned in anaphase (MEN ON), Tem1 primarily localizes to the spindle pole body (SPB,
65 functional equivalent of centrosomes in yeast) that moves into the bud (daughter SPB or dSPB).
66 However, if the spindle is mis-positioned (MEN OFF), Tem1 is largely cytoplasmic.
67 Intriguingly, Tem1 localization to the SPB is highly dynamic with a residence time of around 5
68 s[17,18,20]. Furthermore, forcing Tem1 localization to the SPB by artificially tethering Tem1 to the
69 SPB component Cnm67 overrides the checkpoint (SPoC defective)[20], indicating a functional link
70 between Tem1 localization and MEN activation. How Tem1's nucleotide cycle and localization
71 integrate to regulate MEN activation remains unclear.
72 Here, we demonstrate that Tem1 does not function as a molecular switch as its nucleotide
73 state does not change upon MEN activation. Instead, Tem1's GTP/GDP cycle is used to establish
74 a localization-based concentration difference in the cell: only at the SPB can Tem1 achieve the
75 effective concentration required to interact with its downstream effector protein Cdc15.
76 Consequently, spindle position regulates MEN activation by controlling Tem1 localization. This
77 noncanonical GTPase signaling mechanism differs from the molecular switch paradigm
78 described by Ras and enables Tem1 to couple a spatial cue (i.e., spindle position) to downstream
79 signaling. The observation that localizing a protein to SPB/centrosomes can modulate protein-
80 protein interactions is likely relevant to other localization-based signaling scenarios.
81

82 **RESULTS**

83 ***Tem1 is a noncanonical small GTPase with relatively low affinity for nucleotides.***

84 To understand the role of Tem1's nucleotide cycle, we first characterized the biochemical
85 properties of purified Tem1 (Fig. S1): its intrinsic GTP hydrolysis and nucleotide exchange rates,
86 and nucleotide binding activities. Tem1 hydrolyzed GTP with k_{hyd} = 0.011 ± 0.001 min^{-1} (or 1.8
87 × 10^{-4} s^{-1}, Fig. 1D) and exhibited a nucleotide exchange rate k_{ex} = 0.005 ± 0.0006 s^{-1} (Fig. 1E).
88 The hydrolysis rate is slower than those previously measured with an indirect method[13], whereas
89 the exchange rate is similar to prior reports[11,13] and much faster than that of Ras (Fig. 1E). The
90 fast intrinsic nucleotide exchange rate of Tem1 prompted us to examine whether Tem1 has a
91 reduced affinity for nucleotides. Indeed, we found that Tem1 has a low micromolar affinity for a
92 fluorescent derivative of GDP (MANT-GDP, K_D = 1.2 ± 0.1 μM, Fig. 1F), in contrast to the
93 picomolar to nanomolar nucleotide affinities for typical small GTPases[3]. These results suggest
94 that while the intrinsic GTP hydrolysis rate is low for Tem1, the fast intrinsic nucleotide
95 exchange renders Tem1 a self-activating molecular switch as the OFF state ($Tem1^{GDP}$) is
96 unstable due to the high GTP to GDP ratio in the cell[21]. Consequently, Tem1's nucleotide state is
97 mainly controlled by the GAP activity.

98

99 ***Tem1's effector protein Cdc15 has a weak preference for $Tem1^{GTP}$.***

100 We next examined the interaction between Tem1 and its effector Cdc15. As an effector, we
101 expected Cdc15 to have a strong preference for $Tem1^{GTP}$. To measure the binding affinity
102 between Cdc15 and Tem1 with different nucleotides, we developed an assay using AlphaLISA[22],
103 a bead-based technology that reports on biomolecular interactions. We mixed recombinant
104 biotinylated Tem1 loaded with either GTPγS or GDP with Cdc15-eGFP from yeast lysate. Their
105 interaction was detected with two populations of beads that bind Cdc15 and Tem1, respectively,
106 and produce proximity-based luminescence upon interaction (Fig. 2A). Titrating biotinylated
107 Tem1 promotes AlphaLISA signal until the amount of Tem1 exceeds the bead binding capacity,
108 after which additional Tem1 competes with bead-bound Tem1 and reduces the signal (the hook
109 point, Fig. 2B). This assay revealed that Cdc15 indeed had a higher affinity towards $Tem1^{GTP\gamma S}$
110 but also showed detectable binding towards $Tem1^{GDP}$ prior to the hook point (Fig. 2B). Using a
111 competition binding assay with unlabeled Tem1(Fig. 2D), we estimated the binding affinity of
112 Cdc15 to $Tem1^{GTP\gamma S}$ (K_D = 3.9 ± 0.8 nM) and $Tem1^{GDP}$ (K_D = 16 ± 3 nM).

113 To validate our AlphaLISA results, we performed co-immunoprecipitation assays
114 between Tem1 and Cdc15 in yeast lysates. To examine the effect of nucleotide state, we
115 generated three mutations in Tem1 (Fig. 2G): a hydrolysis mutant, Tem1Q79L (corresponding to
116 RasQ61L), that locks Tem1 in GTP state; a nucleotide-binding mutants, Tem1T34A
117 (corresponding to Ras-S17A in the P loop region), that bias towards the GDP or apo state; and an
118 effector mutant, Tem1T52A (corresponding to Ras-T35A at switch I region), that cannot
119 undergo the confirmation change upon GTP binding necessary for effector recognition and thus
120 essentially appears as "GDP-locked" for effectors. Contrary to classic GTPase effectors which
121 show enhanced interaction with GTP-locked mutants and minimal interaction with GDP-locked
122 and effector mutants, the GTP-locked Tem1Q79L precipitated less Cdc15 than wildtype Tem1
123 and the GDP-locked/apo Tem1T34A and effector mutant Tem1T52A retained considerable
124 affinity for Cdc15 (≥10%, Fig. 2H, Fig. S2B). The observed weak nucleotide preference of
125 Cdc15 is further supported by the AlphaFold2 predicted Cdc15-Tem1 interaction[23] (Fig. S2C)
126 where the binding interface is away from the nucleotide binding pocket of Tem1. We conclude
127 that Cdc15 is a noncanonical GTPase effector protein with a relatively weak preference for
128 $Tem1^{GTP}$ over $Tem1^{GDP}$. This unusual feature poses constrains on how well Tem1 could function
129 as a molecular switch.
130
131 ***The GAP complex Bub2-Bfa1 preferentially binds $Tem1^{GTP}$.***
132 In contrast to the effector Cdc15, the GAP complex showed a strong preference for $Tem1^{GTP\gamma S}$
133 over $Tem1^{GDP}$ with several orders of magnitude difference in affinity in the AlphaLISA assay
134 (Fig. 2C, see 10% bound line): binding of the GAP to $Tem1^{GTP\gamma S}$ was readily detected even with
135 < 0.1 nM biotinylated Tem1, whereas binding of the GAP to $Tem1^{GDP}$ was barely detectable
136 even with 100 nM Tem1. We estimated the binding affinity of the GAP complex to $Tem1^{GTP\gamma S}$
137 with the competition assay (Fig. 2D, $K_D < 0.4 \pm 0.2$ nM, ~10-fold lower than Cdc15). We further
138 dissected the contribution of each GAP subunit to the Tem1 interaction (Fig. 2E-F). Although
139 Bub2 did not interact with Tem1 in the absence of Bfa1, Bfa1 bound similarly to $Tem1^{GTP\gamma S}$ in
140 the presence or absence of Bub2. Interestingly, Bfa1 showed increased affinity for $Tem1^{GDP}$ in
141 the absence of Bub2 prior to the hook point (Fig. 2E), suggesting that Bfa1 alone and the Bub2-
142 Bfa1 complex interact with Tem1 differently.

143 In parallel, we performed co-immunoprecipitation between different Tem1 nucleotide
144 mutants and the GAP (Fig. 2I). As shown previously[11] and consistent with our AlphaLISA
145 results, the GTP-locked Tem1Q79L interacted more strongly with the GAP than wild-type Tem1
146 while the GDP-locked/apo mutant Tem1T34A and the effector mutant Tem1T52A had
147 significantly reduced affinity for the GAP: almost no Bfa1 was pulled down by these Tem1
148 mutations (Figs. 2I & S2B). We conclude that the GAP complex specifically interacts with
149 $Tem1^{GTP}$. Based on their distinct nucleotide preference and sensitivity to mutations in Tem1
150 (Fig. S2B), our results also suggest that Cdc15 and the GAP complex do not share the exact
151 same binding interface on Tem1.
152
153 ***Tem1's nucleotide state regulates its localization.***
154 How nucleotide state regulates Tem1 remains elusive. Given the correlation between Tem1's
155 SPB localization and its activity, we investigated whether Tem1 nucleotide state regulates its
156 cellular localization. To track Tem1 localization in the cell, we developed a N-terminal
157 fluorescent Tem1 fusion (yEGFP-Tem1) that, unlike previous C-terminal fusions[19,24], showed
158 similar expression and activity as wild-type untagged Tem1 (Fig. S3). Tem1 localizes primarily
159 to the dSPB in metaphase and this localization is enhanced upon anaphase onset (which typically
160 coincides with migration of the dSPB into the bud) followed by a decline as cells exit from
161 mitosis (Fig. 3B). As previously reported[11], the GTP-locked Tem1Q79L showed stronger
162 localization to both SPBs throughout metaphase and anaphase (Fig. 3). In contrast, the inactive
163 GDP-locked/apo mutants T34A abolished SPB localization and the effector mutant T52A
164 significantly reduced SPB localization. These results suggest that Tem1's nucleotide state
165 specifies its SPB localization and that only $Tem1^{GTP}$ is recruited to the SPB.
166
167 ***SPB localization of Tem1 depends on the GAP Bub2-Bfa1 and effector Cdc15.***
168 How is $Tem1^{GTP}$ recruited to the SPB? Previous studies showed that SPB localization of Tem1
169 mainly depends on the GAP complex Bub2-Bfa1[10]. Our finding that the GAP specifically
170 interacts with $Tem1^{GTP}$ could explain the nucleotide dependence of Tem1 localization. However,
171 a small pool of Tem1 can localize to the SPB in a GAP-independent manner through an
172 unknown mechanism. Using our yEGFP-Tem1 fusion and quantitative time-lapse microscopy,
173 we compared the localization patterns of Tem1, the GAP component Bfa1, and Tem1's effector

174 protein Cdc15 in the presence or absence of the catalytic subunit of the GAP complex Bub2 (Fig.
175 4A).
176 Bub2 and Bfa1 form a stable complex that localizes to the SPB[10]. The GAP complex
177 preferentially accumulates at the SPB closest to the bud (typically the dSPB) in metaphase. Upon
178 anaphase onset, this asymmetry is exacerbated due to both an increase in localization at the dSPB
179 and active removal of the GAP from the mSPB[17]. The latter outcome is achieved, at least in part,
180 through phosphorylation of Bfa1 by the inhibitory zone protein Kin4[16,17], a kinase that is
181 restricted to the mother cortex and localizes to the mSPB in anaphase[25,26]. Tem1 localization to
182 the SPB resembled the GAP until late anaphase, when Tem1 also localized to the mSPB (Fig.
183 4A, 12-20 min). The effector Cdc15 did not localize to the SPBs until anaphase onset and
184 showed only a moderate bias toward dSPB. Bfa1 does not localize to either SPBs in the absence
185 of Bub2[10] (Fig. 4A). In contrast, Tem1 and Cdc15 showed synchronized and symmetric
186 localization to both SPBs in late anaphase in *bub2Δ* cells (Fig. 4A, Fig. S4A). Similar
187 localization patterns for Tem1 were found in *bfa1Δ* or *bfa1Δbub2Δ* double mutants (Fig. S4B-
188 D). Furthermore, the GTP-locked Tem1Q79L showed a similar localization profile and anaphase
189 progression as wild-type Tem1 in the absence of the GAP (Fig. S4C-D), consistent with our
190 prediction that as a self-activating GTPase, Tem1 is mainly in the GTP-bound state without the
191 GAP.
192 Given the correlated localization between Tem1 and Cdc15 in *bub2Δ* cells, we
193 hypothesized that in the absence of the GAP, Tem1 (mainly $Tem1^{GTP}$) and Cdc15 form a
194 complex that is recruited to the SPB. In this model, Tem1 and Cdc15 localization to the SPB
195 should be interdependent (Fig. 4B). It is well established that Cdc15 localization depends on
196 Tem1[19] (Fig. S5D), leading us to examine the role of Cdc15 in Tem1 localization: we either
197 depleted Cdc15 with the auxin-inducible degron system[27] (Fig. 4C-D) or generated *cdc15Δ*
198 strains kept alive with a hyperactive *DBF2* allele[28] (Fig. S5A-B). In the degron strains, Cdc15
199 depletion was nearly complete and arrested cells in anaphase (Fig. 4C). Tem1 localization to
200 dSPB was not affected by Cdc15 depletion or deletion in *BFA1* cells but was completely
201 dependent on Cdc15 in *bfa1Δ* cells (Figs. 4D, S5A-B). Similar results were observed for
202 Tem1Q79L (Fig. S5C), demonstrating that Tem1 ($Tem1^{GTP}$) cannot localize to the SPB on its
203 own and relies on either the GAP or Cdc15 for recruitment to the SPB.
204

205 ***GAP stimulated GTP hydrolysis drives the fast turnover of Tem1 at the dSPB.***
206 Because the GAP specifically recruits $Tem1^{GTP}$ to the dSPB, we reasoned that the rapid turnover
207 of Tem1 at the SPB observed previously[17,18,20] could be a result of GAP-stimulated GTP
208 hydrolysis and consequent dissociation of $Tem1^{GDP}$. To test this hypothesis, we sought to
209 compare the turnover of wild-type Tem1 and the hydrolysis deficient Tem1Q79L mutant at the
210 dSPB (Fig. 5A) with fluorescence recovery after photobleaching (FRAP) analysis. We depleted
211 Cdc15 to avoid potential interference of Cdc15-mediated SPB localization of Tem1, although we
212 did not observe significant difference for Tem1 dynamics at the dSPB in anaphase cells with or
213 without Cdc15 depletion (Fig. S6A). Inhibiting GTP hydrolysis with Tem1Q79L increased the
214 residence time of Tem1 at the dSPB in anaphase cells from $t_{1/2}$ = 6 (± 2) s to $t_{1/2}$ = 16 (± 7) s (Fig.
215 5B). A similar reduction in Tem1 turnover was observed in cells with a catalytically dead GAP
216 mutant *bub2R85A* (Fig. S6B). Thus, GAP-stimulated GTP hydrolysis drives the rapid turnover of
217 Tem1 at the dSPB. Importantly, this finding allows us to use Tem1 residence time at the dSPB to
218 estimate *in vivo* GAP activity as the difference of turnover rate between Tem1 and Tem1Q79L.
219
220 ***The GAP is not inactivated in anaphase.***
221 It has been proposed that regulation of GAP activity, presumably by Cdc5 phosphorylation of
222 Bfa1 at the SPB[15], could regulate Tem1 in response to spindle position. Testing this hypothesis
223 requires a way to assess Bub2-Bfa1's GAP activity *in vivo*. We can now use Tem1 FRAP
224 analysis to estimate the GAP-stimulated hydrolysis rate k_{hyd} as the difference of SPB turnover
225 rate between Tem1 and Tem1Q79L ($k_{hyd} = \ln 2/t_{1/2}^{Tem1} - \ln 2/t_{1/2}^{Tem1Q79L}$, Fig. 5A) which was 0.07
226 s^{-1}. This is about 400-fold faster than Tem1's intrinsic GTP hydrolysis rate, indicating that the
227 GAP is active in anaphase.
228 If correct anaphase delivery of the dSPB to the bud downregulates GAP activity to
229 promote Tem1 and MEN activation, then Tem1 residence time at the SPB should lengthen in
230 anaphase. This, however, was not the case. Similar to previous reports[17,18,20], we did not observe
231 a significant difference in Tem1's turnover rate at the SPB between metaphase and anaphase
232 (Fig. 5C). As the turnover of Tem1 at dSPB is mainly driven by GAP-stimulated GTP hydrolysis
233 (Fig. 5A-B), this result indicates that Bub2-Bfa1's GAP activity at the SPB is not downregulated
234 in anaphase compared to metaphase as previously suggested.
235

236 ***Tem1's nucleotide state does not change upon MEN activation.***

237 If the GAP is not inactivated in anaphase, does Tem1's nucleotide state (ratio of $Tem1^{GTP}$ to
238 $Tem1^{GDP}$ in the cell) change between metaphase and anaphase? Assuming that Tem1 undergoes
239 spontaneous GEF-independent nucleotide exchange and GAP-stimulated GTPase hydrolysis, the
240 parameters we measured experimentally combined with cellular concentrations of Tem1 and
241 Bub2-Bfa1 from the literature[29] (Fig. S7) allowed us to calculate that < 10% of Tem1 is in the
242 GTP-bound state in the presence of active GAP, whereas 97% of Tem1 is in the GTP-bound
243 state in the absence of the GAP (Fig. S7A). These ratios are predicted to stay the same between
244 metaphase and anaphase given that GAP activity is not downregulated in anaphase.

245 To validate our conclusions, we sought to assess Tem1's nucleotide state directly. Given
246 that the GAP specifically recruits $Tem1^{GTP}$ to the dSPB, we reasoned that the fraction of SPB
247 localized GAP bound to Tem1 should correlate with cellular $Tem1^{GTP}$ level ([$Tem1^{GTP}$]) and thus
248 can serve as an indicator for [$Tem1^{GTP}$] (Fig. 5D). Indeed, the GTP-locked Tem1Q79L showed
249 dramatically enhanced SPB localization (Fig. 3) due to high [$Tem1^{GTP}$]. We quantified the dSPB
250 localization of Bfa1, Tem1, and Tem1Q79L in cells with Cdc15 depleted (Fig. 5E). All three
251 proteins increased dSPB localization upon anaphase onset synchronously due to the
252 redistribution of GAP (Fig. S8). Since Tem1 is more abundant than the GAP complex (~2.5x)[29]
253 and binds the GAP with sub-nanomolar affinity (Fig. 2D), we assumed that Tem1Q79L saturates
254 all the GAP binding sites and could represent the maximum binding capacity. We thus estimated
255 the fraction of GAP bound to Tem1 as the ratio of dSPB intensity of Tem1 to Tem1Q79L which
256 remained steady over the cell cycle (Fig. 5F). These results strongly suggest that the nucleotide
257 state of Tem1 (ratio of [$Tem1^{GTP}$] to [$Tem1^{GDP}$]) is not modulated to control MEN activation and
258 the majority of Tem1 in the cell remains in the GDP-bound state in both metaphase (MEN
259 inactive) and anaphase (MEN active).

260

261 ***Localization of Tem1 to the SPB promotes MEN activation.***

262 If not by changing Tem1's nucleotide state, how does spindle position regulate MEN activation?
263 Given the functional link between SPB localization of Tem1 and MEN activation, we propose
264 that spindle position regulates the MEN by controlling Tem1 localization. To test whether SPB
265 localization of Tem1 directly controls MEN activation, we took advantage of the nucleotide
266 binding mutants of Tem1 that fail to localize to SPB (Fig. 3). We hypothesized that these

267 mutants are lethal due to mis-localization and artificially localizing them to the SPB should
268 restore successful cell division. We tethered yEGFP-Tem1 to the SPB using a GFP nanobody
269 (GFP binding protein, GBP) fused to a SPB outer plaque component Cnm67. This tethering
270 completely rescued the lethality of both *tem1T34A/N* and *tem1T52A* (Fig. 6A). Direct fusion to
271 Cnm67 also rescued an expanded panel of Tem1 mutants (Fig. S9). Furthermore, when Tem1
272 was tethered to the SPB, cells exited from mitosis with similar kinetics regardless of the
273 nucleotide state (Fig. 6B). These results suggest that SPB localization of Tem1 is a key regulated
274 step for MEN activation and that signaling downstream of Tem1 to the effector kinase Cdc15
275 does not require $Tem1^{GTP}$ as long as Tem1 is correctly localized, consistent with the relatively
276 weak nucleotide preference of Cdc15 (Fig. 2).
277
278 ***Concentrating Tem1 in the cytoplasm promotes MEN activation.***
279 As Cdc15's key target Nud1[30] is a core component of the SPB, the main function of Tem1 could
280 be the recruitment of Cdc15 to the SPB. However, in *bub*Δ cells, MEN activation occurs even
281 without the GAP-mediated recruitment of Tem1 to the SPB (Fig. 4A). We proposed that in the
282 absence of the GAP, Tem1 and Cdc15 form a complex in the cytoplasm that can then localize to
283 the SPB. To test whether the MEN can be activated by inducing Tem1-Cdc15 interaction in the
284 cytoplasm, we modulated local concentrations of the localization-defective Tem1T34A by
285 tethering it to homo-oligomers. Cdc15 forms dimers (or multimers)[31] and due to an avidity effect
286 could be sensitive to local concentrations of Tem1. Fusion to a tetrameric tether (HOTag6[32])
287 failed to rescue *tem1T34A* but fusion to a hexamer (HOTag3[32]) partially rescued the lethality
288 (Fig. 6C). Tethering Tem1 to the surface of genetically-encoded multimeric nanoparticles
289 (GEMs, 120mer)[33] fully rescued the lethality of *tem1T34A* to the same degree as tethering to the
290 SPB (Fig. 6C). These findings suggest that a high local concentration of Tem1 is sufficient for
291 MEN activation.
292 Interestingly, Tem1T34A-coated GEMs clustered at the SPBs in a Bfa1-dependent
293 manner (Figs. 6D & S10A), even though Tem1T34A did not localize to the SPB on its own (Fig.
294 3). This may be due to an avidity effect whereby the high density of Tem1T34A on GEMs
295 compensated for the weak affinity of Tem1T34A for Bub2-Bfa1. To concentrate Tem1 away
296 from the SPB, we repeated the GEM tethering experiment in *bfa1Δ* cells where the GEMs
297 remained mostly in the cytoplasm (Fig. 6D & S10A). Under this condition, we observed the

298 same rescuing effect for Tem1 lethal mutations defective in SPB localization (Fig. 6E). These
299 results support a model in which SPB localization of Tem1 activates the MEN by modulating the
300 effective concentration of Tem1 to promote Tem1-Cdc15 interaction and MEN signaling can be
301 initiated in the cytoplasm by locally concentrating Tem1.
302
303 ***SPoC is sensitive to Tem1 concentration.***
304 If spindle position regulates the MEN by modulating Tem1's effective concentration, then
305 increasing the global concentration of Tem1 should allow MEN activation even with a
306 mispositioned spindle. To assess the sensitivity of SPoC to Tem1 concentration, we titrated
307 cellular Tem1 level by introducing extra copies of the *TEM1* gene (Fig. S11A). We then
308 quantified the integrity of the SPoC by depleting both Kar9 and Dyn1 using auxin-inducible
309 degrons to trigger spindle mispositioning[7] (Fig. 7A). Surprisingly, doubling Tem1 level with one
310 extra copy (2x) was enough to compromise the SPoC (Fig. 7A, ~40% SPoC defective). Cells
311 with three extra copies (4x) were 95% SPoC defective (Fig. 7A). Furthermore, the time to exit
312 mitosis in cells with mispositioned spindles decreased as Tem1 level was increased (Fig. 7B)
313 revealing a dose-dependent relationship between Tem1 ($Tem1^{GTP}$) level and MEN
314 hyperactivation. Increasing cellular effective concentrations of Tem1 by local clustering instead
315 of overexpression also bypassed the SPoC (Fig. S11C). Conversely, in cells expressing the GTP-
316 locked Tem1Q79L mutant, lowering Tem1Q79L level with the auxin-inducible degron restored
317 SPoC integrity (Fig. 7C, from 100% SPoC defective to ~15%). These results demonstrate that
318 SPoC is sensitive to cellular effective concentrations of Tem1 ($Tem1^{GTP}$).
319
320 **DISCUSSION**
321 ***Tem1 is a noncanonical GTPase that does not function as a molecular switch.***
322 We showed that Tem1 undergoes GEF-independent nucleotide exchange due to its lower binding
323 affinity for guanine nucleotides (Fig. 1), and that Tem1's effector protein Cdc15 has only a weak
324 preference for $Tem1^{GTP}$ (Fig. 2). This allows GDP-locked/apo Tem1 mutants that are localized to
325 the SPB to activate the MEN. Most importantly, we demonstrated that Tem1's nucleotide state
326 ([$Tem1^{GTP}$] : [$Tem1^{GDP}$]) does not change upon MEN activation (Fig. 5). Our results suggest that
327 Tem1 is regulated by a noncanonical mechanism where Tem1's effective concentration is the
328 key variable controlled by spindle position (Fig. 7D-E). Regulation of small GTPases by other

329 noncanonical mechanisms like protein degradation (rather than changing nucleotide states) has
330 been reported for the oncogene RIT1[34] and the cytoskeleton regulator RhoB in quiescent
331 endothelium[35]. To the best of our knowledge, Tem1 represents a novel example of small
332 GTPases that functions via a non-switch mechanism regulated by changing localization.
333
334 ***SPoC regulates the MEN by modulating effective Tem1 concentration.***
335 We propose a new model for Tem1 regulation and SPoC that relies on a localization-based
336 concentration difference of Tem1 in the cell to regulate Tem1-Cdc15 interaction and MEN
337 activation (Fig. 7D-E). In support of the model, perturbations that increase cellular effective
338 concentrations of Tem1 either by overexpression (Fig. 7A), defective GTP hydrolysis (Fig. 7A-
339 *bfa1Δ*, Fig. 7C-*TEMQ79L*), or local clustering (Fig. S11C) loosen the requirement of SPB
340 localization of Tem1 for MEN activation and compromise the SPoC. Spindle position regulates
341 localization of the Bub2-Bfa1 GAP to control Tem1 localization and concentration. This is
342 achieved, at least in part, through the inhibitory zone protein Kin4 that actively removes the GAP
343 complex from SPB(s) that remain in the mother compartment by phosphorylating Bfa1[16,17].
344 When the spindle is correctly positioned, the dSPB escapes the inhibitory mother compartment
345 leading to the SPB localization of the GAP and Tem1 to trigger MEN activation. However, if the
346 spindle is mispositioned and both SPBs remain in the mother cell, SPB localizations of the GAP
347 and Tem1 are inhibited, keeping the MEN inactive. Decoupling SPB localization from spindle
348 position by either tethering Tem1 or the GAP to the SPB also compromises the SPoC[11,17,20].
349 Finally, Tem1 is imported into the nucleus for degradation after exit from mitosis[36] (Fig. S12)
350 which facilitates MEN inactivation and resets Tem1 concentration for the following cell cycle.
351 It is still an open question exactly how Tem1-Cdc15 interaction leads to MEN activation.
352 Cdc15's kinase activity is not cell cycle regulated[37]. Instead, Cdc15 is thought to be mainly
353 regulated by changing its localization and thus access to its target Nud1 at the SPB. Based on our
354 finding of the GAP-independent SPB localization of Tem1 and Cdc15 (Fig. 4), we favor a model
355 in which Tem1-Cdc15 complex formation promotes a form of active Cdc15 capable of localizing
356 to the SPB. This could explain the previous finding that tethering Tem1 to the plasma membrane
357 (PM) in the absence of the GAP inhibits MEN activation[20]. PM tethering sequesters Tem1 and
358 thus Cdc15 and would prevent Cdc15's access to Nud1. In contrast, when we tethered
359 Tem1T34A to the GEMs, which are free to diffuse in the cytoplasm in the absence of the GAP,

360 activated Cdc15 (presumably in complex with Tem1T34A on the surface of GEMs) localizes to
361 the SPB (Fig. S10B-C) and brings Tem1T34A coated GEMs to the SPB as well (Fig. S10A).
362
363 ***Additional cell cycle regulation on MEN activation.***
364 Our new model for Tem1 regulation explains how SPoC controls MEN activation in response to
365 spindle position. However, Tem1 already localizes to the dSPB in metaphase when the MEN is
366 supposed to be inactive, albeit at a lower level (~50%) than in anaphase when the MEN is
367 activated (Fig. 4A). Notably, Cdc15 does not localize to the SPB until anaphase (Fig. 4A). What
368 is preventing Tem1 from interacting with Cdc15 and activating the MEN in metaphase? Given
369 the sensitivity of MEN activation to Tem1 concentration (Fig. 7A), one possibility is that the
370 two-fold concentration difference of SPB-localized Tem1 observed between metaphase and
371 anaphase is enough to generate different outcomes for MEN activation. However, in diploid
372 yeast with only one copy of *TEM1*, where SPB-localized Tem1 was reduced by ~50% in
373 anaphase (Fig. S11D), MEN activation was not prevented as these cells proceed to exit from
374 mitosis with only a ~3-min delay (Fig. S11D).
375 Another more plausible explanation is that there is an additional layer of regulation on
376 Tem1-Cdc15 interaction that is cell-cycle dependent. It appears that in metaphase, SPB localized
377 Tem1, although above the threshold concentration for Tem1-Cdc15 complex formation, is
378 prevented from interacting with Cdc15. This inhibition is removed in anaphase to promote
379 complex formation and MEN activation. As Tem1 is recruited to the SPB by Bub2-Bfa1 in
380 metaphase (Fig. 4) and Bfa1 interacts with Tem1 on its own in a different manner than in the
381 GAP complex (Fig. 2E), we propose that a likely candidate for the inhibitor of Tem1-Cdc15
382 interaction is Bfa1. In support of this model, overexpression of Bfa1 without its partner Bub2,
383 arrests cells in anaphase[38–40], presumably through inhibiting Tem1-Cdc15 interaction. Future
384 experiments examining the specific binding interactions between Tem1 and Bfa1/Cdc15 will be
385 required to test this hypothesis.
386
387 ***The role of Tem1's GTP/GDP cycle.***
388 Given that the key mode of regulation for Tem1 is by changing effective concentration, why
389 does the system need a GTPase? In other words, what additional benefit might the GTP/GDP
390 cycle provide for Tem1 regulation? Although Cdc15 has a relatively weak preference for GTP-

391 bound Tem1, Tem1^{GTP} still interacts and activates Cdc15 much more efficiently. The GTP/GDP
392 cycle thus provides an additional layer of concentration control to establish a concentration
393 difference in the cell which prevents precocious MEN activation in the cytoplasm while remains
394 primed for prompt MEN activation at the SPB. We found that in the absence of the GTP/GDP
395 cycle with the GTP-locked Tem1Q79L, while it was possible to establish a semi-functional
396 checkpoint by lowering the overall concentration of Tem1 (Fig. 7C), these cells took longer to
397 exit from mitosis once the spindle is correctly positioned (Fig. S11E). Our results titrating Tem1
398 level (Figs. 7A-B, S11D) further indicates that with the GTP/GDP cycle *S. cerevisiae* cells
399 operate with an optimum Tem1 concentration balancing the speed of mitotic exit and the
400 necessary accuracy required for the checkpoint.
401
402 ***Localization/concentration-based signaling mechanism.***
403 Our results support a model where SPB localization regulates Tem1 and MEN signaling by
404 modulating Tem1's effective concentration without changing its nucleotide state (Fig. 7D-E).
405 The localization-based concentration difference of Tem1 could simply be attributed to high local
406 concentration at the SPB and the avidity effect or an indirect mechanism where additional
407 regulators at the SPB increase Tem1's effective concentration. Our successful attempt in
408 mimicking the concentration effect of SPB localization with the GEMs suggests that high local
409 concentration is at least sufficient to initiate MEN signaling. The concentration effect we
410 observed for Tem1 could be a general mechanism applicable to other localization-based
411 signaling scenarios such as DNA damage response[41] and kinetochore assembly[42]. We speculate
412 that the same mechanism we described for Tem1 is conserved beyond budding yeast and could
413 apply to other small GTPases. Future studies are needed to examine these possibilities.
414

ACKNOWLEDGEMENTS

We thank E Unal (Berkeley, USA), J Haber (Waltham, USA), T Schwartz (Cambridge, USA), A Keating (Cambridge, USA), F Monje-Casas (Sevilla, Spain), S Piatti (Montpellier, France), and L Holt (New York, USA) for strains and reagents; A Murray and D Lew for their critical reading of the manuscript. This work was supported by National Institute of General Medical Science (K99GM140212 to XZ) and the Eunice Kennedy Shriver National Institute of Child Health and Human Development (HD085866 to AA). AA and SB were also investigators of the Howard Hughes Medical Institute.

AUTHOR CONTRIBUTIONS

X.Z. and A.A. conceived the study. X.Z. performed all experiments. S.Y.W. generated Tem1 and Bub2 point mutants. X.Z. wrote the manuscript with input from S.P.B..

COMPETING INTERESTS

The authors declare no competing interests.

431 **MATERIALS AND METHODS**

432 ***Construction of Yeast strains and plasmids***

433 All *Saccharomyces cerevisiae* yeast strains used in this study are derivatives of W303 (A2587)
434 and are listed in Table S1. All plasmids used in this study are listed in Table S2. Yeast cells were
435 cultured in standard YEP media (1% yeast extract, 2% peptone) with 2% D-glucose, or in
436 standard Synthetic Complete media (SC) with 2% D-glucose. Cells were cultured at 25°C unless
437 noted otherwise. C-terminal fusions and deletions were constructed using standard PCR-based
438 methods. N-terminal tagging and point mutations of Tem1 and Bub2 were introduced at the
439 endogenous locus using Cas9-mediated gene editing as described previously[43,44]. Successfully
440 edited clones were checked by PCR and sequencing. Point mutations in GFP and small insertions
441 in the tagging plasmids were introduced via Q5 site-directed mutagenesis. GFP and RFP
442 (mCherry) nanobodies (GBP and RBP) were synthesized as gBlocks and inserted into tagging
443 plasmids via Gibson assembly.

444

445 ***Purification of Tem1 and biotinylated Tem1***

446 Recombinant Tem1 was expressed as a 14xHis-SUMO fusion (p2579) in *Escherichia coli*
447 Rosetta2(DE3) cells. Protein production was induced with 0.3 mM IPTG at 14 °C for 16-20
448 hours. Cells were collected by centrifugation at 6,000 x g, resuspended in lysis buffer (50 mM
449 HEPES, pH 8.0, 500 mM NaCl, 2 mM $MgCl_2$, 25 mM imidazole, 3 mM 2-mercaptoethanol
450 (βME)) supplemented with cOmplete™ EDTA free protease inhibitor cocktail, treated with
451 lysozyme for 30 mins at 4 °C followed by sonication. The lysate was cleared by centrifugation at
452 16,000 x g for 30 min. The soluble fraction was incubated with Ni-NTA agarose (QIAGEN) for
453 1 hour at 4 °C. The resin was washed with lysis buffer and transferred to low imidazole buffer
454 (20 mM HEPES pH 8.0, 100 mM NaCl, 100 mM imidazole, 2 mM $MgCl_2$) along with 2.5 µg
455 SENP protease (gift from T. Schwartz's lab[45]) and incubated at 4 °C overnight. Then the flow
456 through containing the cleaved Tem1 was collected along with a 2 CV wash with low imidazole
457 buffer and loaded onto a Mono S column equilibrated with buffer A (20 mM HEPES pH 8.0, 50
458 mM NaCl, 5 mM $MgCl_2$, 10% glycerol, 1 mM DTT). After washing with buffer A, Tem1 was
459 eluted with a linear gradient from 0 to 100% buffer B (20 mM HEPES pH 8.0, 1 M NaCl, 5 mM
460 $MgCl_2$, 10% glycerol, 1 mM DTT) in 20 CV. To make apo-Tem1, buffer EDTA (20 mM HEPES

461 pH 8.0, 50 mM NaCl, 5 mM EDTA, 10% glycerol, 1 mM DTT) was used before elution to
462 remove nucleotides bound to Tem1. Tem1 peak fractions were pooled and concentrated.
463 To generate biotinylated Tem1, Tem1 was expressed as a AviTag-6xHis fusion together
464 with BirA (p3034, based on pDW363[46]) in *Escherichia coli* Rosetta2(DE3) cells. Protein
465 production was induced with 0.5 mM IPTG at 16 °C in 1L LB supplemented with 15 mg biotin
466 for 16-20 hours. Cells were collected and process as described above, and the soluble fraction
467 was incubated with Ni-NTA agarose (QIAGEN) for 1 hour at 4 °C. The resin was washed with
468 lysis buffer followed by low imidazole buffer (20 mM HEPES pH 8.0, 100 mM NaCl, 25 mM
469 imidazole, 5 mM $MgCl_2$) and biotinylated Tem1 was eluted with high imidazole buffer (20 mM
470 HEPES pH 8.0, 100 mM NaCl, 250 mM imidazole, 5 mM $MgCl_2$) and loaded onto a Mono S
471 column for additional purification (see above). Tem1 peak fractions were pooled and
472 concentrated.
473
474 ***GTPase assay***
475 GTP hydrolysis was measured for recombinant Tem1 with [α-^{32}P]-GTP. Tem1 (3.3 μM final
476 concentration) was mixed with GTP (33 μM final) supplemented with 5 μCi [α-^{32}P]-GTP
477 (PerkinElmer) in the reaction buffer (20 mM HEPES pH 7.5, 25 mM NaCl, 5 mM $MgCl_2$) on ice
478 and the reaction was initiated by shifting to 30 ºC. At indicated time intervals, 2 μl reaction was
479 removed and quenched with quench buffer (50 mM EDTA, 2% SDS) and analyzed via thin layer
480 chromatography (TLC) on PEI-cellulose plates (Millipore sigma 105579). The plates were
481 developed in 0.75M KH_2PO_4 (pH 3.5) and dried plates were exposed to storage phosphor screens
482 overnight and scanned on a Typhoon phosphorimager (Cytiva). It is worth noting that when
483 optimizing assay conditions, we found that EDTA which is often included in GTPase assays for
484 small GTPase to increase nucleotide exchange or turnover did not make a difference in the rate
485 of GTP hydrolysis for Tem1, consistent with Tem1's high intrinsic nucleotide exchange rate.
486
487 ***Nucleotide exchange and binding assay***
488 To load Tem1 with fluorescently labeled nucleotides (i.e., MANT-GDP) for nucleotide exchange
489 assays, recombinant Tem1 was first diluted in Tem1 dilution buffer (20 mM HEPES pH 7.5, 100
490 mM NaCl, 5mM $MgCl_2$, 10% glycerol, 0.2 mg/ml BSA, 2 mM DTT) to 10 μM and mixed with
491 equal volume of 400 nM MANT-GDP or MANT-GTP/GTPγS in Tem1 binding buffer (20 mM

492 HEPES pH 7.5, 100 mM NaCl, 5mM $MgCl_2$). The mixture was incubated for at least 10 minutes
493 at room temperature to reach equilibrium and then kept on ice. Three technical replicates of 18 µl
494 MANT-GDP/GTP/GTPγS loaded Tem1 mixture were plated in a black 384-well nonbinding
495 microplate (Greiner Bio-One) and read in a SpectraMax ID5 plate reader (Molecular Dynamics)
496 at 30 ºC. To initiate nucleotide exchange, 2 µl of 10 mM unlabeled nucleotide (i.e., GTP) was
497 added (1 mM final concentration) and readings were taken at 30s interval with 355 nm excitation
498 and 448 nm emission. k_{obs} was measured by fitting a single exponential decay after background
499 subtraction.
500 To measure binding affinities, apo-Tem1 was diluted with Tem1 dilution buffer first to
501 40 µM then 2-fold serial diluted 10 times with the dilution buffer. Equal volumes of 400 nM
502 MANT-GDP or MANT-GTPγS in Tem1 binding buffer were mixed with the apo-Tem1 dilution
503 series and 15 µl of each mixture was placed in a black 384-well nonbinding microplate (Greiner
504 Bio-One) and read in a SpectraMax ID5 plate reader (Molecular Dynamics) after 30 minutes
505 incubation at 30 ºC. Three independent dilutions were performed for each nucleotide conditions.
506 K_D was measured by fitting a quadratic equation:
507 $y = y_{max}\left(L + P + K_D - \sqrt{(L + P + K_D)^2 - 4LP}\right)/2L$, where y_{max} is the maximum
508 fluorescence signal at saturated binding, L is the total ligand concentration (MANT-GDP/GTPγS,
509 0.2 µM), P is total Tem1 concentration.
510
511 ***Microscopy and image analysis***
512 For live-cell microscopy, cells were imaged on agarose pads (2% agarose in SC medium + 2%
513 glucose, unless otherwise noted) affixed to a glass slide and covered with a coverslip. Imaging
514 was performed on a DeltaVision Elite platform (GE Healthcare Bio-Sciences) with an InsightSSI
515 solid state light source, an UltimateFocus hardware autofocus system and a model IX-71,
516 Olympus microscope controlled by SoftWoRx software. A 60x Plan APO 1.42NA objective and
517 CoolSNAP HQ2 camera were used for image acquisition. For each time point, 8 *z* sections with
518 0.75 µm spacing were collect for each channel and were deconvolved. Maximum projections of
519 the deconvolved *z* stack were used for fluorescence quantification.
520 Image analysis was performed with custom scripts in MATLAB as described previously.
521 First, yeast cells were segmented and tracked through time using the bright-field image stacks.

522 Next, fluorescence images of cell cycle markers (such as Spc42 or NLS) were segmented and
523 tracked based on cell segmentation. Appearance of a cell cycle marker in a cell during the
524 acquisition period was used to identify buds (daughter cells) and cell division events. Tracking of
525 the cell cycle markers that migrated into the buds were used to identify the corresponding mother
526 cells. Finally, for each division event identified, localization of the target protein at regions
527 defined by the cell cycle markers was quantified.
528 For localization at the SPBs (I_{SPB}), maximum intensity of the target protein at SPBs
529 (based on segmentation of Spc42) was used given that the size of SPBs (~100 nm) is within the
530 diffraction limit of light microscopy. To calculate the relative enrichment of target protein at the
531 SPB, intensities were normalized to the median intensity in the cytosol: $I_{SPB}/I_{cytosol} - 1$. Single
532 cell traces were aligned based on the timing of anaphase onset or the movement of a SPB into the
533 bud as indicated in figures, and averaged. 95% confidence intervals were calculated as $\mu \pm$
534 $1.96 * \sigma/\sqrt{n}$, where μ and σ denote the mean and standard deviation respectively and n is the
535 number of cells measured.
536
537 ***Spotting assays***
538 Tem1 mutants were constructed in the native locus with CRISPR in y3059 carrying a
539 hyperactive Dbf2. Correct mutants were then crossed with y2892 (*tem1* knockout carrying a
540 URA3-based CEN covering plasmid expressing wild-type Tem1) to generate strains with Tem1
541 mutants and the covering plasmid. Additional alleles tested were also introduced via cross. For
542 spotting assays, these strains were grown in YPD overnight and diluted to OD 0.2 in YPD and
543 grow for at least one doubling at room temperature. 5-fold serial dilutions were made for each
544 culture starting from OD 0.2 and 4 µl were spotted onto YPD or plates with 5'-fluoroorotic acid
545 (5-FOA) which selects cells that are viable after losing the URA3 covering plasmid.
546
547 ***Immunoblot analysis***
548 Log-phase cultures of cells grown in YEP + 2% glucose were harvested and treated with
549 5% TCA at 4°C overnight. TCA treated cell pellets were washed with acetone, air dried, and
550 resuspended in lysis buffer (10 mM Tris, 1 mM EDTA, 2.75 mM DTT, pH = 8). Cells were
551 lysed by bead-beating using a Multivortexer (max speed, 20 minutes) and glass beads at 4°C and
552 followed by boiling in SDS PAGE protein loading buffer for 5 minutes. Lysates were clarified

553 by centrifugation and were resolved with NuPAGE 4-12% Bis-Tris protein gel (Thermo Fisher
554 Scientific) prior to transfer onto nitrocellulose membranes. Tem1 was detected with an anti-
555 Tem1 antibody generated in rabbit against the peptide CKKLTIPEINEIGDPLLIYKHL[24] at a
556 1:300 dilution. GFP was detected using an anti-GFP antibody (Clontech, JL-8) at a 1:1000
557 dilution. Myc tags were detected using an anti-Myc antibody (abcam, 9E10) at a 1:500 dilution.
558 V5 tags were detected using an anti-V5 antibody (Invitrogen) at a 1:2000 dilution. HA tags were
559 detected with an anti-HA.11 antibody (BioLegend) at 1:1000 dilution. Clb2 was detected using a
560 rabbit anti-Clb2 at 1:1000 dilution. Kar2 was detected using a rabbit anti-Kar2 antiserum at a
561 1:200,000 dilution. DyLight 800 conjugated secondary antibodies (Cell Signaling) were used at a
562 1 :10,000 dilution. Blots were imaged using the ChemiDoc MP imager system (BioRad).
563
564 ***Co-immunoprecipitation analysis***
565 Log-phase cultures (~ 40 OD of cells) were harvested and snap frozen in liquid nitrogen. Cell
566 pellets were thawed in lysis buffer (50 mM Tris pH=7.5, 150mM NaCl, 1% NP40, 5mM MgCl2,
567 1mM DTT, supplemented with cOmplete™ EDTA free protease inhibitor and PhosSTOP™
568 inhibitor) and lysed via bead-beating with silica beads in a FastPrep-24™ (MP Biomedicals).
569 Lysates were clarified by centrifugation and protein concentration in the lysates was measured
570 with Bradford assay (Bio-Rad). 15 µl of GFP-Trap agarose (ChromoTek) was washed three
571 times with NP40 buffer (50 mM Tris pH=7.5, 150mM NaCl, 1% NP40, 5mM MgCl2) and
572 incubated with clarified lysates containing ~3 mg of total protein per sample for 1 hour at 4 ºC.
573 The agarose beads were washed five times with NP40 buffer. Afterwards, the bound proteins
574 were eluted by boiling the beads in protein loading buffer and resolved on NuPAGE 4–12% Bis-
575 Tris protein gels (Thermo Fisher Scientific) followed by immunoblot analysis (see above).
576
577 ***AlphaLISA analysis***
578 Purified biotinylated Tem1 was first diluted to 500 nM and incubated with 100 µM GTPγS or
579 GDP in assay buffer (50 mM Tris pH=7.5, 150mM NaCl, 1% NP40, 5mM MgCl2, 1mM DTT,
580 1x cOmplete™ EDTA free protease inhibitor and PhosSTOP™ inhibitor, 0.1% BSA) and 3-fold
581 serial diluted. Equal volume of 100 µg/ml (5x final concentration) Alphascreen Streptavidin
582 Donor beads (PerkinElmer 6760002S) diluted in assay buffer were added and incubated with
583 nucleotide loaded Tem1 for 1 hour at room temperature in the dark. Log-phase cultures (~ 10

584 OD of cells) containing eGFP tagged Bub2/Bfa1/Cdc15 were harvested and snap frozen in liquid
585 nitrogen. Cell pellets were processed as described for co-immunoprecipitation assays and diluted
586 to 3 mg/ml total protein concentration with lysis buffer. 5 µl lysate was added to each 384 well
587 Alpha plates (PerkinElmer) together with 10 µl Tem1 coated donor beads and 10 µl 50 µg/µl
588 AlphaLISA Anti-GFP Acceptor Beads (PerkinElmer AL133C) diluted in assay buffer. The plate
589 was incubated for 4-6 hours at 4 ºC and read using a M1000 plate reader (Tecan) with the default
590 AlphaScreen settings at room temperature. Alpha signals were analyzed by first subtracting
591 background signal measured with control yeast lysate without eGFP (y1584) and then
592 normalized with the maximum signal of each experiment. For the competition assays with
593 unlabeled Tem1, 0.5 nM and 5 nM final concentration of biotinylated Tem1 were used for the
594 GTPγS and GDP binding assays respectively.
595
596 ***FRAP analysis***
597 FRAP analysis was performed on a DeltaVision-OMX Super-Resolution Microscope (Applied
598 Precision, GE Healthcare Bio-Sciences) using a 60x oil objective and a 488 nm laser adjusted to
599 bleach an area of approximately 0.5 µm in radius. Two prebleach images were acquired followed
600 by a laser pulse (50% intensity) of 0.02 s duration and postbleach images were acquired at 1
601 s/frame for 60 s. Images at each time points were maximum projections of 5 *z* stacks with 0.5 µm
602 spacing. Images were analyzed with a custom MATLAB script. After subtracting the
603 background, fluorescence intensities in the cytosol, $I_{cytosol}(t)$, and at the SPB, $I_{SPB}(t)$ were
604 measured after segmenting the cell and SPBs. Photobleaching was corrected by normalizing I_{SPB}
605 (t) with $I_{cytosol}(t)$, $I_{SPB_norm}(t) = I_{SPB}(t) / I_{cytosol}(t)$. Double normalization for FRAP was calculated
606 to scale the photobleaching effect between 0 and 1: $I_{SPB_FRAP}(t) = [I_{SPB_norm}(t) - I_{SPB_norm}(0)] /$
607 $[I_{SPB_norm}(pre) - I_{SPB_norm}(0)]$, where $t = 0$ is the time point (frame) right after photobleaching and
608 $t = pre$ is the time point (frame) right before photobleaching. The double normalized FRAP
609 curves were then fitted to a single exponential curve: $y = y_{max}\left(1 - e^{\left(-ln2/t_{1/2}\right)t}\right)$, where y_{max}
610 is the fraction recovered while $t_{1/2}$ is the half-recovery time.
611
612 ***SPoC assay***

613 Spindle mispositioning was induced by depleting both Kar9 and Dyn1 with the auxin-inducible
614 degron system. Spindle position and checkpoint integrity was monitored with fluorescently
615 labeled α-tubulin (GFP-Tub1 or mCherry-Tub1). Cells were imaged on agarose pads (2%
616 agarose in SC medium + 2% glucose + 100 μM IAA) as described in Microscopy at 5 min
617 interval for 4 to 5 hours. Images were analyzed by scoring the following 4 categories: spindle
618 elongated in the mother cell and the cell was arrested in anaphase with elongated spindle (1),
619 spindle elongated in the mother cell and the cell exited mitosis with spindle disassembled in the
620 mother cell (2), spindle elongated in the mother cell but later extended into the bud and exited
621 mitosis with one spindle pole in the bud (3), and spindle elongated into the bud and exited
622 mitosis with one spindle pole in the bud (4). Only categories 1&2 were used to calculate the
623 percentages of cells arrested vs exited in mother.
624
625 ***Modeling Tem1's nucleotide cycle***
626 Virtual Cell software (VCell[47,48]) version 7.5.0 was used to model Tem1's nucleotide cycle. The
627 model, "Tem1_Bfa1" by user "xiaoxuez", can be accessed within the VCell software (available
628 at https://vcell.org). Two compartments (cytosol and SPB) were set up for the GAP stimulated
629 GTP hydrolysis and GEF-independent nucleotide exchange where the GAP (represented in the
630 model as "Bfa1") was placed at SPB to simulate anaphase cells. We have also simulated
631 metaphase cells by distributing the GAP evenly between the cytosol and SPB and found no
632 difference in the results. Each simulation started with 25 nM $Tem1^{GTP}$ (~ 1500 molecules/cell) in
633 the cytosol and ran for 300 s to reach steady state. The parameters used can be found in the
634 online model and the parameters scanned are summarized in Fig. S7B.
635
636
637

638 **REFERENCES**

639 1. Wennerberg, K. The Ras superfamily at a glance. *J. Cell Sci.* **118**, 843–846 (2005).

640 2. Vetter, I. R. & Wittinghofer, A. The Guanine Nucleotide-Binding Switch in Three
641 Dimensions. *Science* **294**, 1299–1304 (2001).

642 3. Bos, J. L., Rehmann, H. & Wittinghofer, A. GEFs and GAPs: Critical Elements in the
643 Control of Small G Proteins. *Cell* **129**, 865–877 (2007).

644 4. Simanshu, D. K., Nissley, D. V. & McCormick, F. RAS Proteins and Their Regulators in
645 Human Disease. *Cell* **170**, 17–33 (2017).

646 5. Guertin, D. A., Trautmann, S. & McCollum, D. Cytokinesis in Eukaryotes. *Microbiol. Mol.*
647 *Biol. Rev.* **66**, 155–178 (2002).

648 6. Chan, L. Y. & Amon, A. Spindle Position Is Coordinated with Cell-Cycle Progression
649 through Establishment of Mitotic Exit-Activating and -Inhibitory Zones. *Mol. Cell* **39**, 444–
650 454 (2010).

651 7. Falk, J. E. *et al.* Spatial signals link exit from mitosis to spindle position. *eLife* **5**, e14036
652 (2016).

653 8. Campbell, I. W., Zhou, X. & Amon, A. The Mitotic Exit Network integrates temporal and
654 spatial signals by distributing regulation across multiple components. *eLife* **8**, (2019).

655 9. Bardin, A. J., Visintin, R. & Amon, A. A Mechanism for Coupling Exit from Mitosis to
656 Partitioning of the Nucleus. *Cell* **102**, 21–31 (2000).

657 10. Pereira, G., Höfken, T., Grindlay, J., Manson, C. & Schiebel, E. The Bub2p Spindle
658 Checkpoint Links Nuclear Migration with Mitotic Exit. *Mol. Cell* **6**, 1–10 (2000).

659 11. Scarfone, I. *et al.* Asymmetry of the Budding Yeast Tem1 GTPase at Spindle Poles Is
660 Required for Spindle Positioning But Not for Mitotic Exit. *PLOS Genet.* **11**, e1004938
661 (2015).

662 12. Asakawa, K., Yoshida, S., Otake, F. & Toh-e, A. A novel functional domain of Cdc15 kinase
663 is required for its interaction with Tem1 GTPase in Saccharomyces cerevisiae. *Genetics* **157**,
664 1437–1450 (2001).
665 13. Geymonat, M. *et al.* Control of Mitotic Exit in Budding Yeast. *J. Biol. Chem.* **277**, 28439–
666 28445 (2002).
667 14. Hu, F. *et al.* Regulation of the Bub2/Bfa1 GAP Complex by Cdc5 and Cell Cycle
668 Checkpoints. *Cell* **107**, 655–665 (2001).
669 15. Geymonat, M., Spanos, A., Walker, P. A., Johnston, L. H. & Sedgwick, S. G. *In Vitro*
670 Regulation of Budding Yeast Bfa1/Bub2 GAP Activity by Cdc5. *J. Biol. Chem.* **278**, 14591–
671 14594 (2003).
672 16. Maekawa, H., Priest, C., Lechner, J., Pereira, G. & Schiebel, E. The yeast centrosome
673 translates the positional information of the anaphase spindle into a cell cycle signal. *J. Cell*
674 *Biol.* **179**, 423–436 (2007).
675 17. Caydasi, A. K. & Pereira, G. Spindle Alignment Regulates the Dynamic Association of
676 Checkpoint Proteins with Yeast Spindle Pole Bodies. *Dev. Cell* **16**, 146–156 (2009).
677 18. Molk, J. N. *et al.* The Differential Roles of Budding Yeast Tem1p, Cdc15p, and Bub2p
678 Protein Dynamics in Mitotic Exit□D□V. *Mol. Biol. Cell* **15**, (2004).
679 19. Campbell, I. W., Zhou, X. & Amon, A. Spindle pole bodies function as signal amplifiers in
680 the Mitotic Exit Network. *Mol. Biol. Cell* **31**, 906–916 (2020).
681 20. Valerio-Santiago, M. & Monje-Casas, F. Tem1 localization to the spindle pole bodies is
682 essential for mitotic exit and impairs spindle checkpoint function. *J. Cell Biol.* **192**, 599–614
683 (2011).

684 21. Rudoni, S., Colombo, S., Coccetti, P. & Martegani, E. Role of guanine nucleotides in the
685 regulation of the Ras/cAMP pathway in *Saccharomyces cerevisiae*. *Biochim. Biophys. Acta*
686 *BBA - Mol. Cell Res.* **1538**, 181–189 (2001).
687 22. Beaudet, L. *et al.* AlphaLISA immunoassays: the no-wash alternative to ELISAs for research
688 and drug discovery. *Nat. Methods* **5**, an8–an9 (2008).
689 23. Humphreys, I. R. *et al.* Computed structures of core eukaryotic protein complexes. *Science*
690 **374**, eabm4805 (2021).
691 24. Chan, L. Y. & Amon, A. The protein phosphatase 2A functions in the spindle position
692 checkpoint by regulating the checkpoint kinase Kin4. *Genes Dev.* **23**, 1639–1649 (2009).
693 25. D'Aquino, K. E. *et al.* The Protein Kinase Kin4 Inhibits Exit from Mitosis in Response to
694 Spindle Position Defects. *Mol. Cell* **19**, 223–234 (2005).
695 26. Pereira, G. & Schiebel, E. Kin4 Kinase Delays Mitotic Exit in Response to Spindle
696 Alignment Defects. *Mol. Cell* **19**, 209–221 (2005).
697 27. Morawska, M. & Ulrich, H. D. An expanded tool kit for the auxin-inducible degron system
698 in budding yeast. *Yeast Chichester Engl.* **30**, 341–351 (2013).
699 28. Geymonat, M., Spanos, A., de Bettignies, G. & Sedgwick, S. G. Lte1 contributes to Bfa1
700 localization rather than stimulating nucleotide exchange by Tem1. *J. Cell Biol.* **187**, 497–511
701 (2009).
702 29. Caydasi, A. K. *et al.* A dynamical model of the spindle position checkpoint. *Mol. Syst. Biol.*
703 **8**, 582 (2012).
704 30. Rock, J. M. *et al.* Activation of the Yeast Hippo Pathway by Phosphorylation-Dependent
705 Assembly of Signaling Complexes. *Science* **340**, 871–875 (2013).

706 31. Bardin, A. J., Boselli, M. G. & Amon, A. Mitotic Exit Regulation through Distinct Domains
707 within the Protein Kinase Cdc15. *Mol. Cell. Biol.* **23**, 5018–5030 (2003).
708 32. Zhang, Q. *et al.* Visualizing Dynamics of Cell Signaling In Vivo with a Phase Separation-
709 Based Kinase Reporter. *Mol. Cell* **69**, 334-346.e4 (2018).
710 33. Delarue, M. *et al.* mTORC1 Controls Phase Separation and the Biophysical Properties of the
711 Cytoplasm by Tuning Crowding. *Cell* **174**, 338-349.e20 (2018).
712 34. Castel, P. *et al.* RIT1 oncoproteins escape LZTR1-mediated proteolysis. *Science* **363**, 1226–
713 1230 (2019).
714 35. Podieh, F. *et al.* Differential role for rapid proteostasis in Rho GTPase-mediated control of
715 quiescent endothelial integrity. *J. Biol. Chem.* **299**, 104593 (2023).
716 36. Devault, A. & Piatti, S. Downregulation of the Tem1 GTPase by Amn1 after cytokinesis
717 involves both nuclear import and SCF-mediated degradation. *J. Cell Sci.* **134**, jcs258972
718 (2021).
719 37. Jaspersen, S. L. & Morgan, D. O. Cdc14 activates Cdc15 to promote mitotic exit in budding
720 yeast. *Curr. Biol.* **10**, 615–618 (2000).
721 38. Ro, H.-S., Song, S. & Lee, K. S. Bfa1 can regulate Tem1 function independently of Bub2 in
722 the mitotic exit network of Saccharomyces cerevisiae. *Proc. Natl. Acad. Sci.* **99**, 5436–5441
723 (2002).
724 39. Whalen, J., Sniffen, C., Gartland, S., Vannini, M. & Seshan, A. Budding Yeast BFA1 Has
725 Multiple Positive Roles in Directing Late Mitotic Events. *G3 GenesGenomesGenetics* **8**,
726 3397–3410 (2018).
727 40. Li, Y. & Song, K. The N-Terminal Domain of Bfa1 Coordinates Mitotic Exit Independent of
728 GAP Activity in Saccharomyces cerevisiae. *Cells* **11**, 2179 (2022).

729 41. Ruis, K., Huynh, O., Montales, K., Barr, N. A. & Michael, W. M. Delineation of a minimal
730 topoisomerase II binding protein 1 for regulated activation of ATR at DNA double-strand
731 breaks. *J. Biol. Chem.* **298**, (2022).
732 42. Sissoko, G. B., Tarasovetc, E. V., Marescal, O., Grishchuk, E. L. & Cheeseman, I. M.
733 Higher-order protein assembly controls kinetochore formation. *Nat. Cell Biol.* **26**, 45–56
734 (2024).
735 43. Zhou, X., Li, W., Liu, Y. & Amon, A. Cross-compartment signal propagation in the mitotic
736 exit network. *eLife* **10**, e63645 (2021).
737 44. Anand, R., Memisoglu, G. & Haber, J. Cas9-mediated gene editing in Saccharomyces
738 cerevisiae. *Protoc. Exch.* (2017) doi:10.1038/protex.2017.021a.
739 45. Nordeen, S. A., Turman, D. L. & Schwartz, T. U. Yeast Nup84-Nup133 complex structure
740 details flexibility and reveals conservation of the membrane anchoring ALPS motif. *Nat.*
741 *Commun.* **11**, 6060 (2020).
742 46. Tsao, K.-L., Debarbieri, B., Michel, H. & Waugh, D. S. A versatile plasmid expression
743 vector for the production of biotinylated proteins by site-specific, enzymatic modification in
744 *Escherichia coli*. *Gene* **169**, 59–64 (1996).
745 47. Schaff, J., Fink, C. C., Slepchenko, B., Carson, J. H. & Loew, L. M. A general computational
746 framework for modeling cellular structure and function. *Biophys. J.* **73**, 1135–1146 (1997).
747 48. Cowan, A. E., Moraru, I. I., Schaff, J. C., Slepchenko, B. M. & Loew, L. M. Chapter 8 -
748 Spatial Modeling of Cell Signaling Networks. in *Methods in Cell Biology* (eds. Asthagiri, A.
749 R. & Arkin, A. P.) vol. 110 195–221 (Academic Press, 2012).
750
751

Figure 1: Tem1 is a noncanonical GTPase with relatively low affinity to nucleotides.

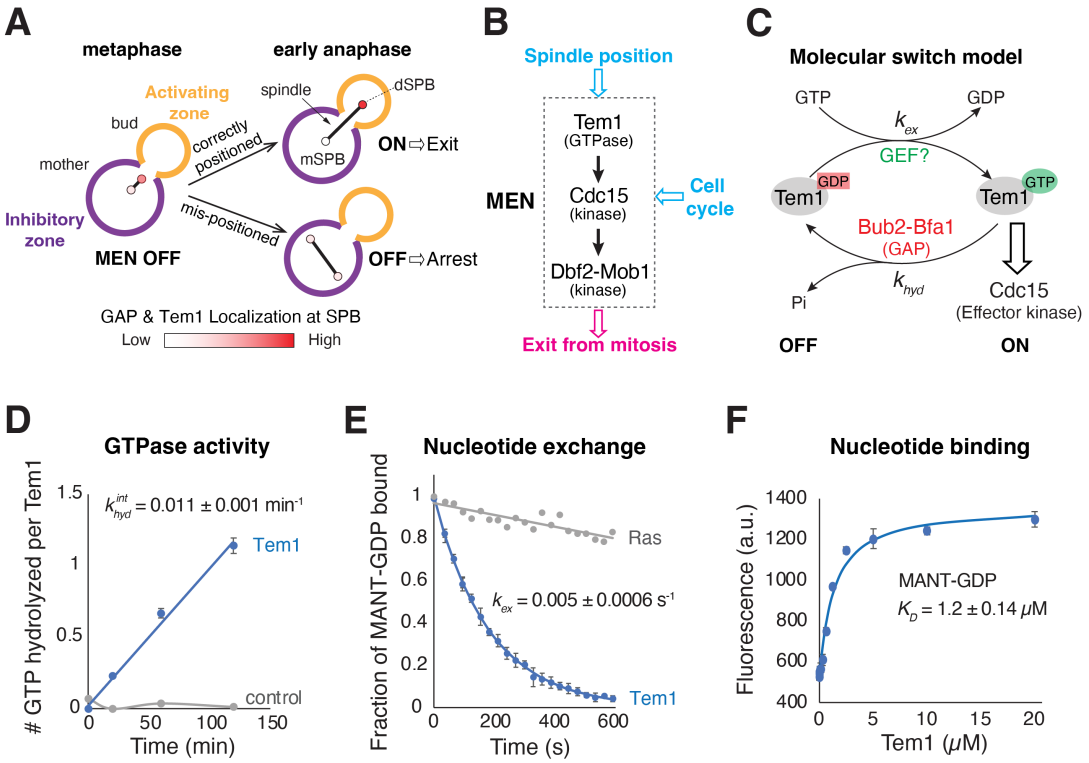

(**A**) Illustration of the spindle position checkpoint in budding yeast and localization of the MEN GTPase Tem1 and its GAP.

(**B**) Major components of the MEN and its inputs and outputs.

(**C**) Molecular switch model for Tem1.

(**D**) GTPase activity of Tem1. Recombinantly purified Tem1 was mixed with GTP and [α-^{32}P]GTP on ice and the reaction was initiated by shifting to 30 °C. Samples were taken at indicated time points and analyzed by TLC (Fig. S1B-C). Shown are the average of 3 technical replicates with a linear fit. Error bars represent ± standard deviation (SD).

(**E**) The rate of nucleotide exchange (MANT-GDP to GTP) for Tem1 and N-Ras. Recombinantly purified Tem1 (5 μM) and N-Ras (5 μM) were first incubated with MANT-GDP (200 nM) and the nucleotide exchange was initiated by the addition of excess GTP (1 mM). Shown are the average of 3 technical replicates with an exponential fit for Tem1 and a linear fit for N-Ras. Error bars represent ± SD.

(**F**) The binding affinity of Tem1 for MANT-GDP. 200 nM MANT-GDP was titrated with increasing amount of purified apo-Tem1. Shown are the average from 3 technical replicates with a quadratic fit for the dissociation constant (K_D). Error bars represent ± SD.

Figure 2: Tem1's effector Cdc15 has a weak preference for Tem1^{GTP}.

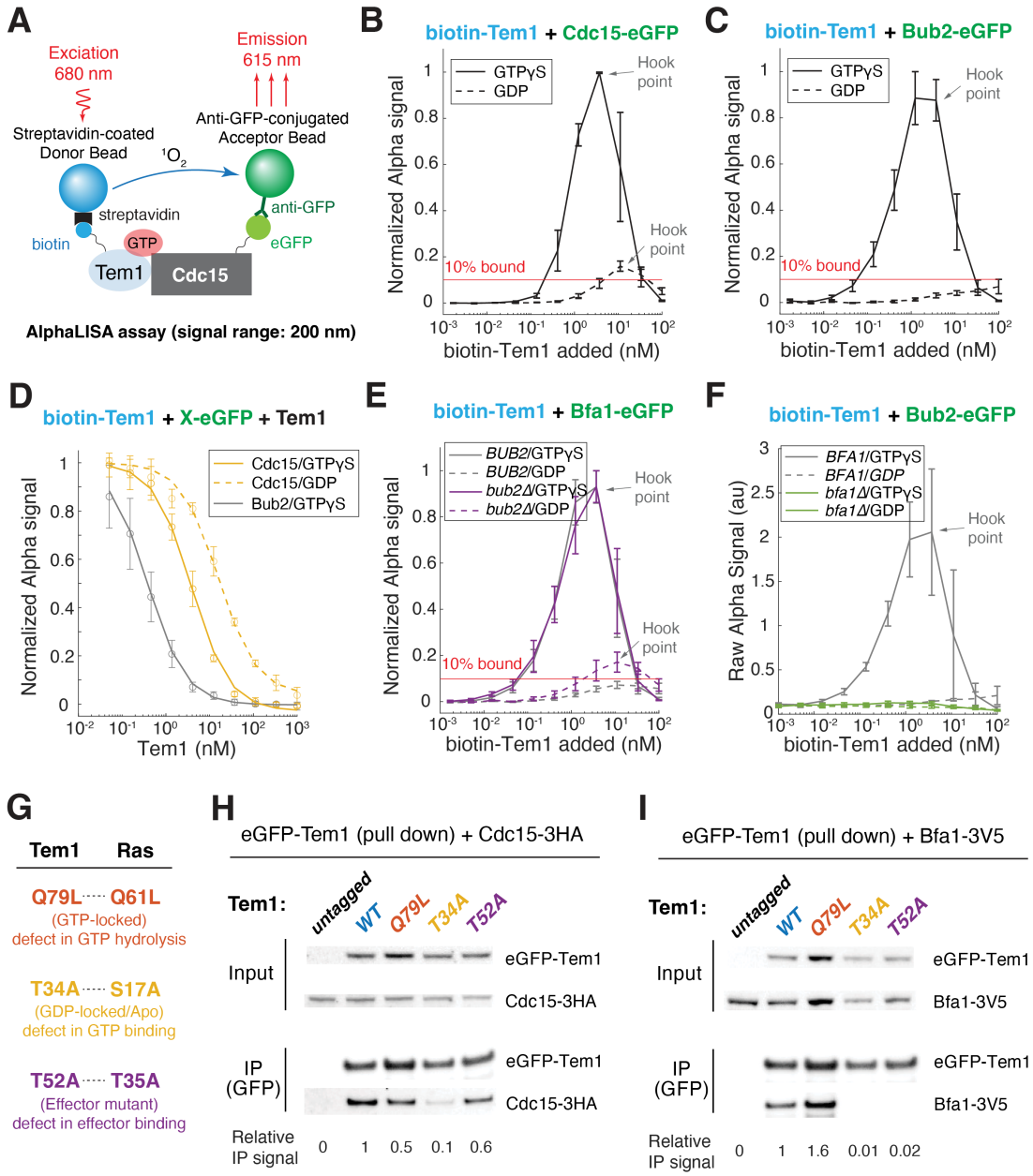

(**A**) Illustration of the hybrid AlphaLISA assay used in this study. Recombinant biotinylated Tem1 were incubated together with cell lysate with eGFP tagged binding partners in the presence of GTPγS or GDP. The interaction was monitored with streptavidin coated Alpha donor beads and anti-GFP conjugated accepter beads.

(**B-C**) Interaction between recombinant biotinylated Tem1 and eGFP tagged Cdc15 (B) or Bub2 (C) in lysate monitored by AlphaLISA. Diluted lysate of y1275 (Cdc15-eGFP) or y1378 (Bub2-eGFP) were incubated with different concentrations of recombinant biotinylated Tem1 in the

presence of GTPγS or GDP. The Alpha signals were normalized to the maximum signal of each sample in the GTPγS condition. Black lines represent the average of three biological replicates and error bars denote standard deviation (SD). The Hook point is when the added biotin-Tem1 exceeds the binding capacity of the Alpha Donor beads which results in a competition between biotin-Tem1 in solution and on beads for binding. Red line indicates 10% of the available eGFP tagged protein (maximum binding capacity defined by the GTPγS condition) were bound by biotin-Tem1 on beads.

(**D**) Dissociation constant of Tem1 binding to Cdc15 and the GAP estimated by a competition binding assay. Diluted lysate of y1275 (Cdc15-eGFP) or y1378 (Bub2-eGFP) were incubated with a fixed amount of biotinylated Tem1 and different concentrations of unlabeled Tem1 in the presence of GTPγS or GDP. Signal for Bub2-eGFP with GDP was too low to be quantified reliably. The Alpha signals were double normalized to the signal without competing Tem1 (normalized signal = 1) and without biotin-Tem1 (normalized signal = 0). Lines represent the average of three biological replicates and error bars denote SD.

(**E-F**) Interaction between biotinylated Tem1 and eGFP tagged Bfa1 (E) or Bub2 (F). Diluted lysate of y1374 (Bfa1-eGFP), y1378 (Bub2-eGFP), y3099 (Bfa1-eGFP in *bub2Δ*), or y3632 (Bub2-eGFP in *bfa1Δ*) were incubated with different concentrations of biotinylated Tem1 in the presence of GTPγS or GDP, and the interaction was monitored with AlphaLISA. Lines represent the average of three biological replicates and error bars denote SD.

(**G**) Point mutations generated in this study to modulate Tem1's nucleotide state.

(**H-I**) Interaction between different Tem1 mutants and the effector Cdc15 (H) or GAP complex (I) via co-immunoprecipitation. yEGFP-Tem1 was immunoprecipitated from exponentially grown cells of the indicated genotypes (y3461/y3452/y3472/y3457/y3456 or y2761/y2885/y2886/y3209/y3208) and the presence of Bfa1-3V5 or Cdc15-3HA were analyzed by Western blot analysis.

Figure 3: Tem1's Nucleotide state regulates its localization.

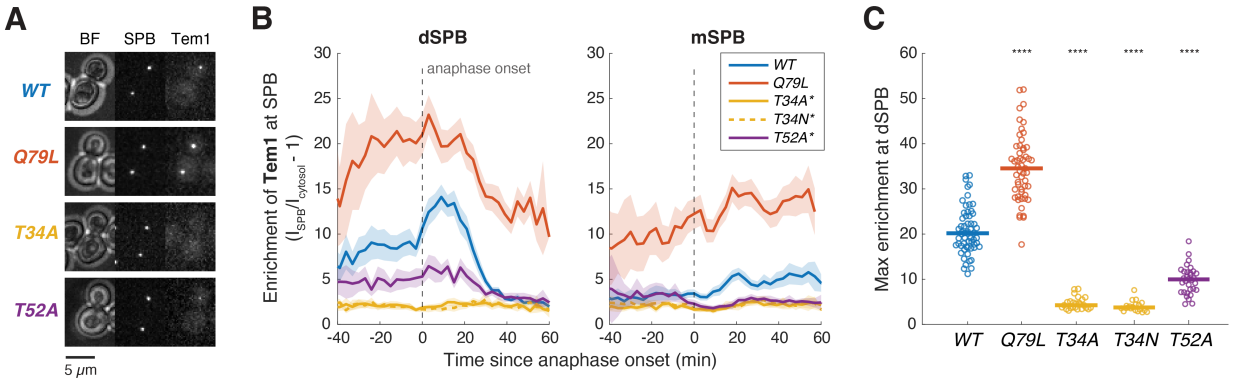

(**A-C**) Representative images and quantification of SPB localization in cells expressing yEGFP tagged wild-type Tem1 (y1748, n = 73 cells), GTP-locked hydrolysis mutant Q79L (y1824, n = 63 cells), GDP-locked/apo nucleotide binding mutant T34A/N (y3167/y3171, n = 29/21 cells), or effector binding mutant T52A (y3147, n = 32 cells) together with Spc42-mScarlet-I (SPB marker). Cells expressing *tem1T34A/N* and *tem1T52A* (marked with *) were kept alive with hyperactive *DBF2-HyA* that can rescue *tem1Δ*. Cells were grown at 25°C in SC medium + 2% glucose and imaged every 3 minutes for 4 hours. Single cell traces were aligned based on anaphase onset, as defined as spindle length > 3 μm (measured based on SPB marker Spc42-mScarlet-I), and averaged. Solid lines represent the mean, shaded areas represent 95% confidence intervals (B). For maximum enrichment at SPB (C), solid lines represent the median. ****$p < 0.0001$ by two-sided Wilcoxon rank sum test for comparing with *WT*.

Figure 4: Localization of Tem1 to the SPB depends on its GAP and effector.

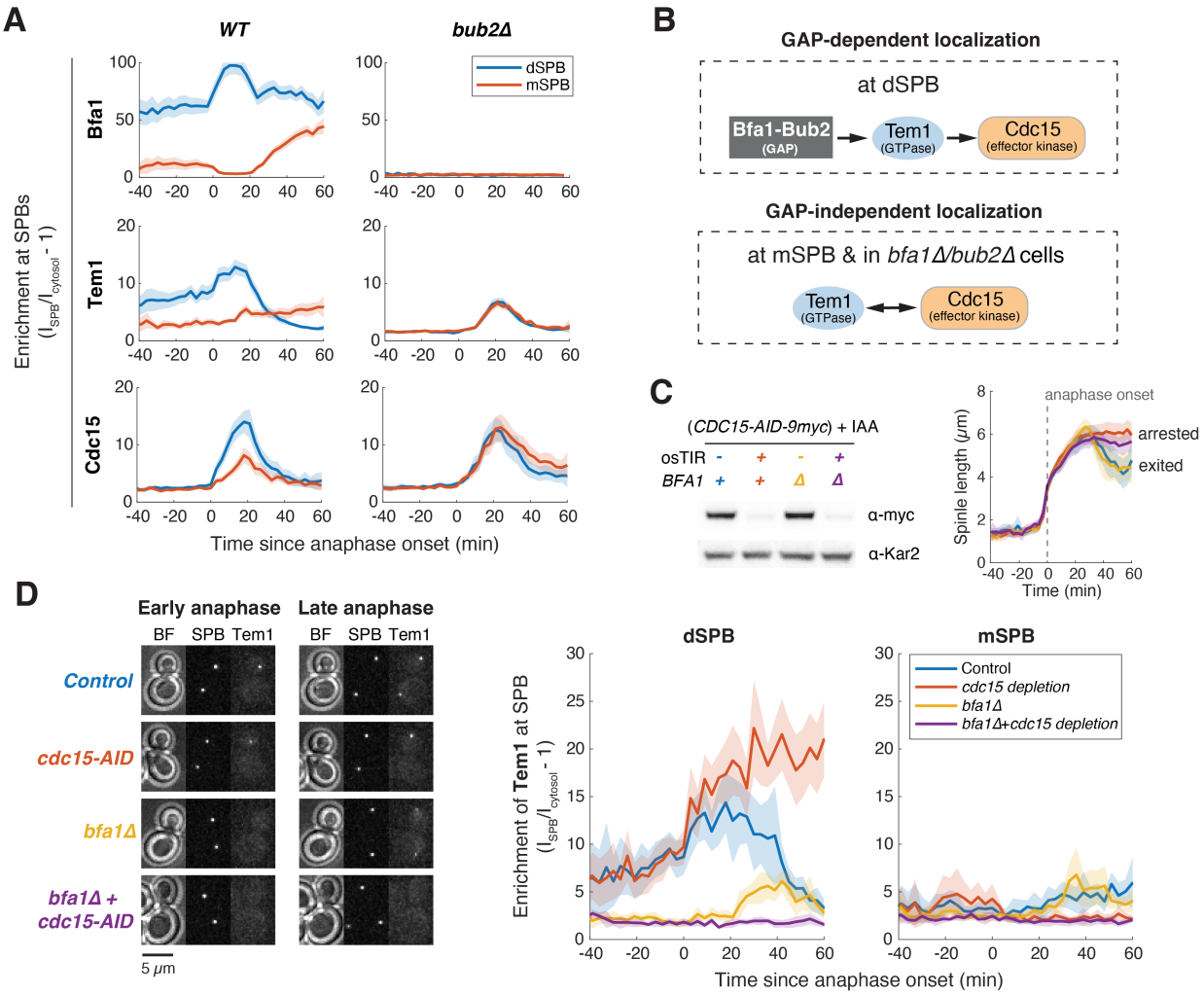

(**A**) Comparison of SPB localization for Bfa1, Tem1 and Cdc15 with or without *BUB2*. Cells with the indicated *BUB2* alleles (columns) and yEGFP-labeled proteins (rows) were grown at 25 °C in SC medium + 2% glucose and imaged every 3 minutes for 4 hours. Strains imaged were y1374 (Bfa1-yEGFP, *n* = 104 cells), y3099 (Bfa1-yEGFP in *bub2Δ*, *n* = 17 cells), y1748 (yEGFP-Tem1, *n* = 65 cells), y1929 (yEGFP-Tem1 in *bub2Δ*, *n* = 72 cells), y1275 (Cdc15-yEGFP, *n* = 79 cells), and y1693 (Cdc15-yEGFP in *bub2Δ*, *n* = 76 cells).

(**B**) Dependency of SPB localization for two different modes of localization patterns observed.

(**C**) Cdc15 was efficiently depleted with the auxin-inducible degron (*CDC15-AID*). Cells with the indicated genotypes (y3229 (*osTIR-/BFA1*), y3224 (*osTIR+/BFA1*), y3228 (*osTIR-/bfa1Δ*), y3223 (*osTIR+/ bfa1Δ*)) were grown at 25 °C in SC medium + 2% glucose + 200 μM IAA for 2 hours before harvesting for Western blot analysis (left). Anaphase progression (right) was

monitored in these cells by measuring spindle length (distance between two SPBs). Cells with Cdc15 depleted arrested in anaphase with elongated spindles whereas non-depleted cells disassembled their spindle (as indicated by the shortening of the distance between SPBs in late anaphase) to exit from mitosis.

(**D**) Representative images (left) and quantification (right) of Tem1 localization at the SPB with or without depleting Cdc15 (*CDC15-AID* +/- *osTIR*) in the presence or absence of *BFA1*. Cells of y3229 (Tem1 control, n = 16 cells), y3224 (Tem1 with Cdc15 depletion, n = 16 cells), y3228 (Tem1 in *bfa1Δ*, n = 12 cells), y3223 (Tem1 in *bfa1Δ* with Cdc15 depletion, n = 10 cells) were grown at 25 °C in SC medium + 2% glucose + 200 μM auxin IAA and imaged every 3 minutes for 4 hours.

For all graphs, single cell traces were aligned based on anaphase onset, as defined in Fig. 3, and averaged. Solid lines represent the average. Shaded areas represent 95% confidence intervals.

Figure 5: Tem1's nucleotide state does not change upon MEN activation.

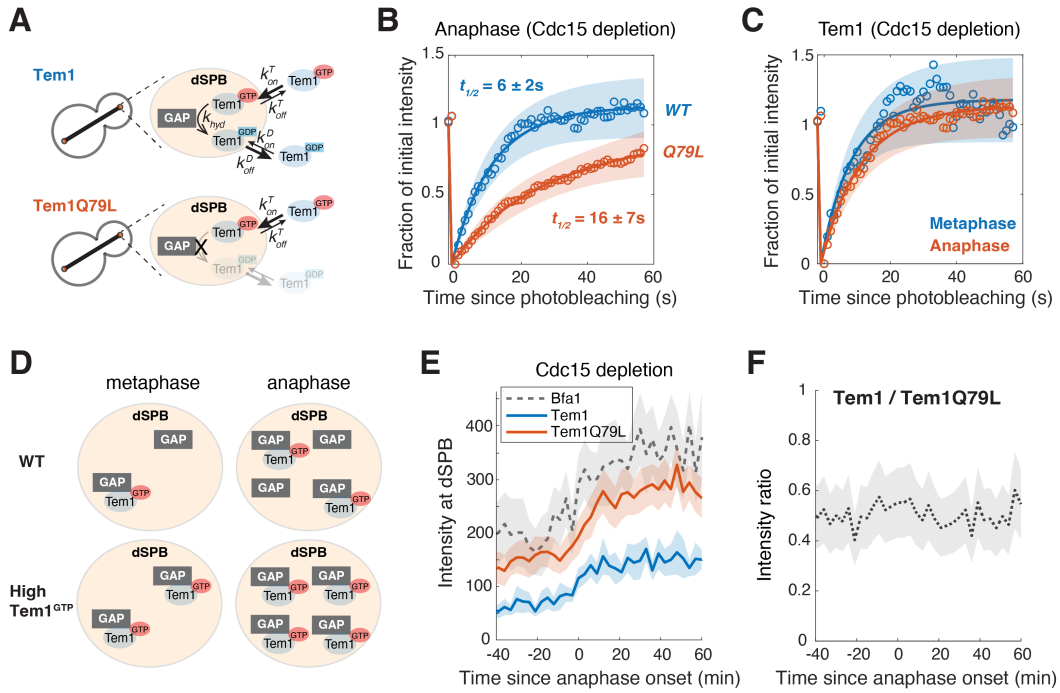

(**A**) Illustration of the different routes for Tem1 and the GTP-locked Tem1Q79L at dSPB. Once $Tem1^{GTP}$ is recruited to the dSPB by the GAP, its departure can occur either via $Tem1^{GTP}$ dissociation (k_{off}^{T}) or GAP-stimulated GTP hydrolysis (k_{hyd}) followed by dissociation (k_{off}^{D}). Assuming $k_{off}^{D} >> k_{hyd}$, the residence time of Tem1 at the dSPB ($t_{1/2}^{Tem1}$) is set by the sum of two rates: $t_{1/2}^{Tem1} = \ln 2/(k_{off}^{T} + k_{hyd})$. For Tem1Q79L, its residence time ($t_{1/2}^{Tem1Q79L}$) is simply $t_{1/2}^{Tem1Q79L} = \ln 2/k_{off}^{T}$ assuming that $Tem1^{GTP}$ and Tem1Q79L dissociate at similar rates.

(**B**) FRAP analysis of Tem1 and TemQ79L at dSPB in anaphase. Cells of y3900 (*TEM1*, $n = 9$ cells) and y3903 (*TEM1Q79L*, $n = 15$ cells) were grown and imaged at room temperature in SC medium + 2% glucose + 100 μM IAA. Circles represent the average normalized fluorescence intensities after correcting for photo-bleaching during acquisition. Solid lines are the average fit and shaded areas represent SD. Half recovery time $t_{1/2} \pm$ SD are indicated.

(**C**) FRAP analysis of Tem1 at dSPB in metaphase and anaphase. Cells of y3900 were grown and imaged at room temperature in SC medium + 2% glucose + 100 μM IAA.

(**D**) Proposed model for GAP and Tem1 localization at the SPB. Under wildtype condition (low [$Tem1^{GTP}$] in the cell), only a fraction of the GAP complex at the dSPB is bound to $Tem1^{GTP}$ in both metaphase and anaphase. While more GAP complex is recruited to dSPB in anaphase, the fraction of GAP bound to $Tem1^{GTP}$ does not change between metaphase and anaphase. In cells

with high [Tem1^{GTP}] such as with *TEM1Q79L*, most of the GAP complex are bound to [Tem1^{GTP}] because Tem1 is more abundant than the GAP.

(**E**) dSPB localization of Tem1 (*WT* or *Q79L*) and Bfa1 in cells with Cdc15 depleted. Cells of y3900 (Tem1, *n* = 16 cells), y3903 (Tem1Q79L, *n* = 35 cells), and y4123 (Bfa1, *n* = 24 cells) were grown at 25 °C in SC medium + 2% glucose + 100 μM IAA and imaged every 3 minutes for 4 hours. Lines represent the average. Shaded areas represent 95% confidence intervals.

(**F**) Ratio of dSPB intensities of Tem1 to Tem1Q79L from (E) was plotted to estimate the cellular level of Tem1^{GTP}.

Figure 6: SPB localization modulates effective concentration of Tem1 for MEN activation.

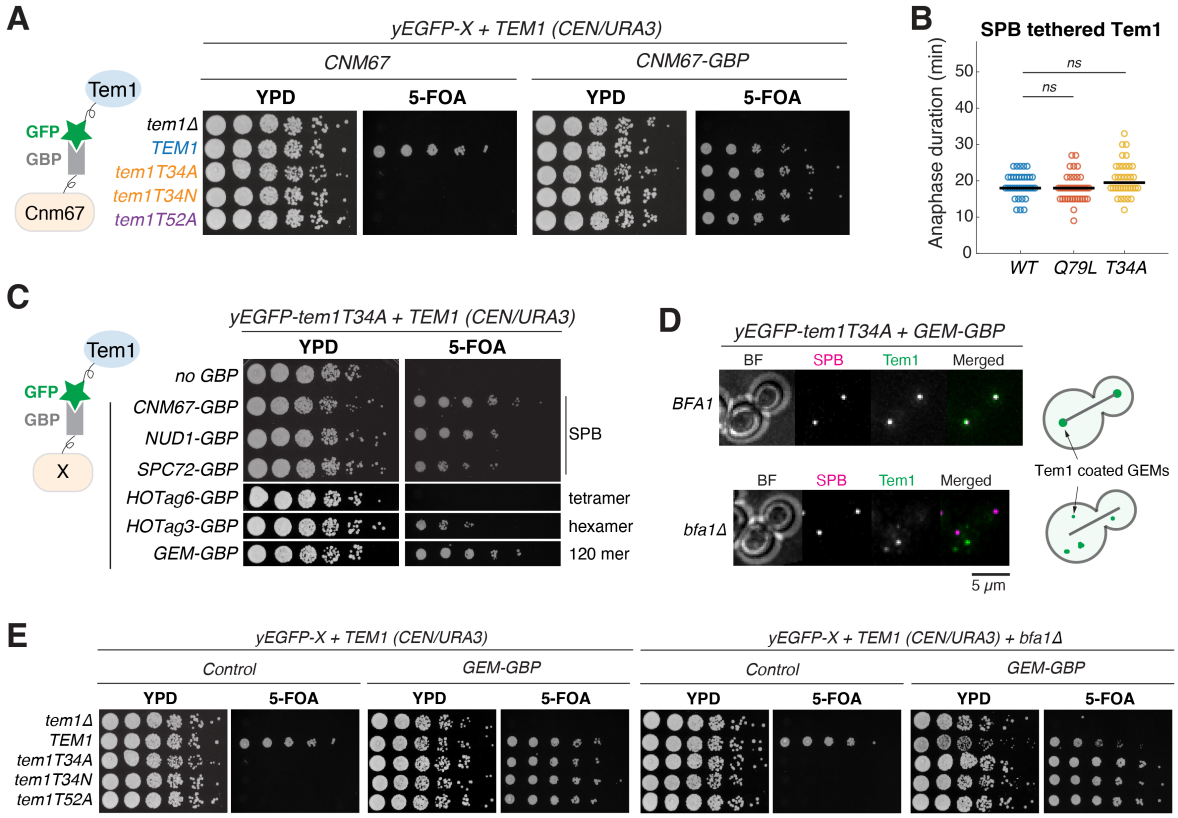

(**A**) Complementation analysis of Tem1 mutants with or without tethering to the SPB via *CNM67-GBP*. 5-fold serial dilutions of strains y2891/y3202/y3203/y3204/y3214 and y3303/y3304/y3305/y3306/y3310, with the indicated *TEM1* alleles, were spotted onto plates with or without 5'-fluoroorotic acid (5-FOA) and incubated at 25°C for 2 to 3 days. The presence of 5-FOA selects cells that are viable after losing the *TEM1 (URA3/CEN)* plasmid. GBP = GFP binding protein.

(**B**) Distribution of anaphase duration for different *yEGFP-TEM1* alleles in the presence of *CNM67-GBP* (y3289, y3287, and y3291; *n* =46, 43, and 47 cells respectively). Cells were grown at 25°C in SC medium + 2% glucose and imaged every 3 minutes for 4 hours. Solid lines represent the median.

(**C**) Complementation analysis of *tem1T34A* with and without tethering to different GBP fusion proteins. 5-fold serial dilutions of strains y3203/y3305/y3500/y3499/y3958/y3956/y3502 were spotted onto plates with or without 5-FOA and incubated at 25°C for 2 to 3 days.

(**D**) Representative localization of GEM-tethered Tem1T34A in the presence or absence of *BFA1*. Cells of y3630 and y3557 were grown at 25 °C in SC medium + 2% glucose and imaged every 3 minutes for 4 hours.

(**E**) Complementation analysis of different Tem1 mutants tethered to GEMs in the presence or absence of *BFA1*. 5-fold serial dilutions of strains y2891/y3202/y3203/y3204/y3214, y3970/y3973/y3502/y3976/y3985, y3971/y3974/y3948/y3977/y3986, and y3972/y3975/y3945/y3978/y3987 were spotted onto plates with or without 5-FOA and incubated at 25°C for 2 to 3 days.

Figure 7: SPoC is sensitive to Tem1 concentration.

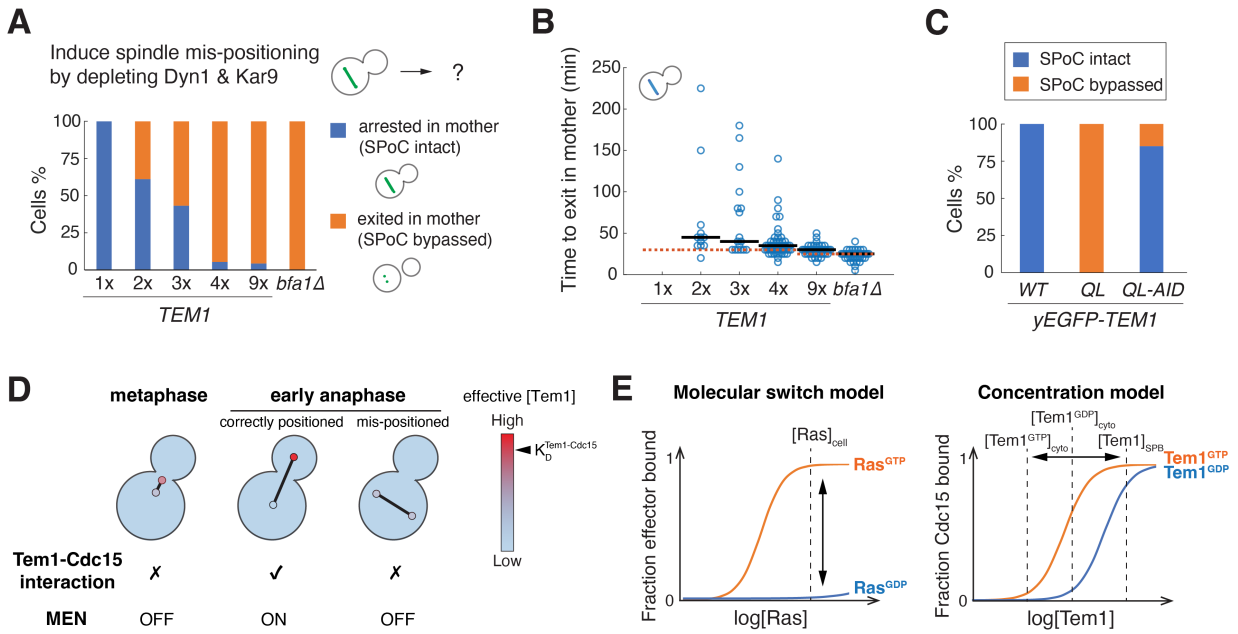

(**A-B**) Evaluation of SPoC integrity in cells with different amount of Tem1. Cells of y3733 (1x*TEM1*, *n* = 102 cells), y3729 (2x*TEM1*, *n* = 72 cells), y3816 (3x*TEM1*, *n* = 64 cells), y3730 (4x*TEM1*, *n* = 102 cells), y3732 (9x*TEM1*, *n* = 101 cells), and y3815 (*bfa1Δ*, *n* = 65 cells) were grown at 25 °C in SC medium + 2% glucose + 100 µM IAA to induce spindle mispositioning by depleting Dyn1 and Kar9 and imaged every 5 minutes for 5 hours. Status of the spindle and cell cycle stages were monitored with GFP-Tub1. For time to exit in mother (mispositioned spindle disassembled in the mother cell) in D, solid lines represent the median, red dashed line indicate the median time to exit in bud (normal anaphase progression with correctly positioned spindle).

(**C**) Evaluation of SPoC integrity in cells expressing Tem1Q79L. Cells of y3817 (yEGFP-*TEM1*, *n* = 55 cells), y3818 (yEGFP-*TEM1Q79L*, *n* = 47 cells), and y4311 (yEGFP-*TEM1Q79L-AID**, *n* = 108 cells) were grown and monitored as described in (A).

(**D**) Proposed model for Tem1 regulation.

(**E**) Comparison between the canonical molecular switch model for Ras and the concentration model for Tem1.

Figure S1: Biochemical characterization of Tem1.

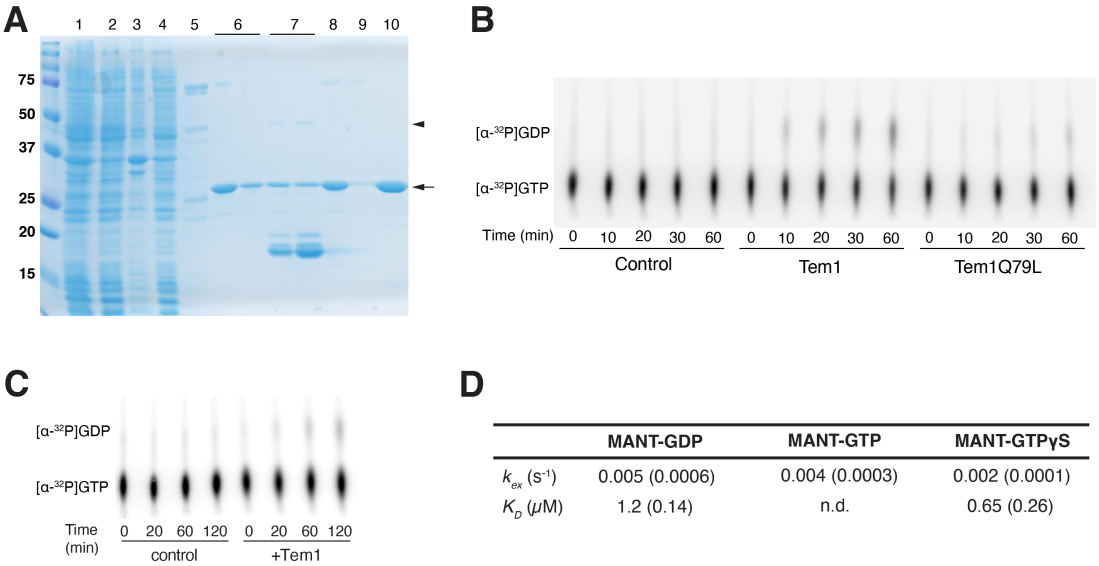

	MANT-GDP	MANT-GTP	MANT-GTPγS
k_{ex} (s^{-1})	0.005 (0.0006)	0.004 (0.0003)	0.002 (0.0001)
K_D (μM)	1.2 (0.14)	n.d.	0.65 (0.26)

(**A**) Purification of Tem1. Tem1 was expressed in *E. coli* as a 14xHis-SUMO-Tem1 fusion with p2579. *Lane 1*, lysate; *lane 2*, soluble fraction; *lane 3*, insoluble fraction; *lane 4*, flowthrough of Ni-NTA column; *lane 5*, wash with lysis buffer; *lane 6*, elution after overnight digest with SENP protease which contains cleaved Tem1; *lane 7*, elution with high imidazole buffer where the remaining 14xHis-SUMO and uncut fusion protein were eluted; *lane 8*, input for Mono S column; *lane 9*, wash with buffer A; *lane 10*, combined peak elution of Tem1 from Mono S. Arrowhead marks 14xHis-SUMO-Tem1 fusion (41 kDa) and arrow marks Tem1 (27 kDa).
(**B-C**) Representative raw thin layer chromatography (TLC) results for measuring GTPase activity of recombinantly purified Tem1 and the hydrolysis deficient mutant Tem1Q79L. No protein was added to the control sample (buffer only).
(**D**) Summary of biochemical properties of Tem1 *in vitro*. Shown are the averages of three independent experiments and SD in parentheses. n.d., not determined (due to GTP hydrolysis). The difference of the observed exchange rate between MANT-GTP ($k_{obs} \approx k_{off}$ (GTP) + $k_{hydrolysis}$) and MANT-GTPγS ($k_{obs} \approx k_{off}$ (GTPγS)) is likely not driven by GTP hydrolysis as previously assumed in filter-binding assays because GTP hydrolysis occurs at a rate an order of magnitude slower than dissociation ($k_{obs} \sim 10^{-3}$ s^{-1}, while $k_{hydrolysis} \sim 10^{-4}$ s^{-1}). Rather, we propose that the observed rates reflect differences in affinity or off rate of the nucleotides ($k_{obs} \approx k_{off}$, when $k_{hydrolysis} << k_{obs}$). The higher affinity for MANT-GTPγS relative to MANT-GDP is consistent with the lower exchange rate for MANT-GTPγS we observed.

Figure S2: Interaction between Tem1 and Cdc15 or the GAP complex.

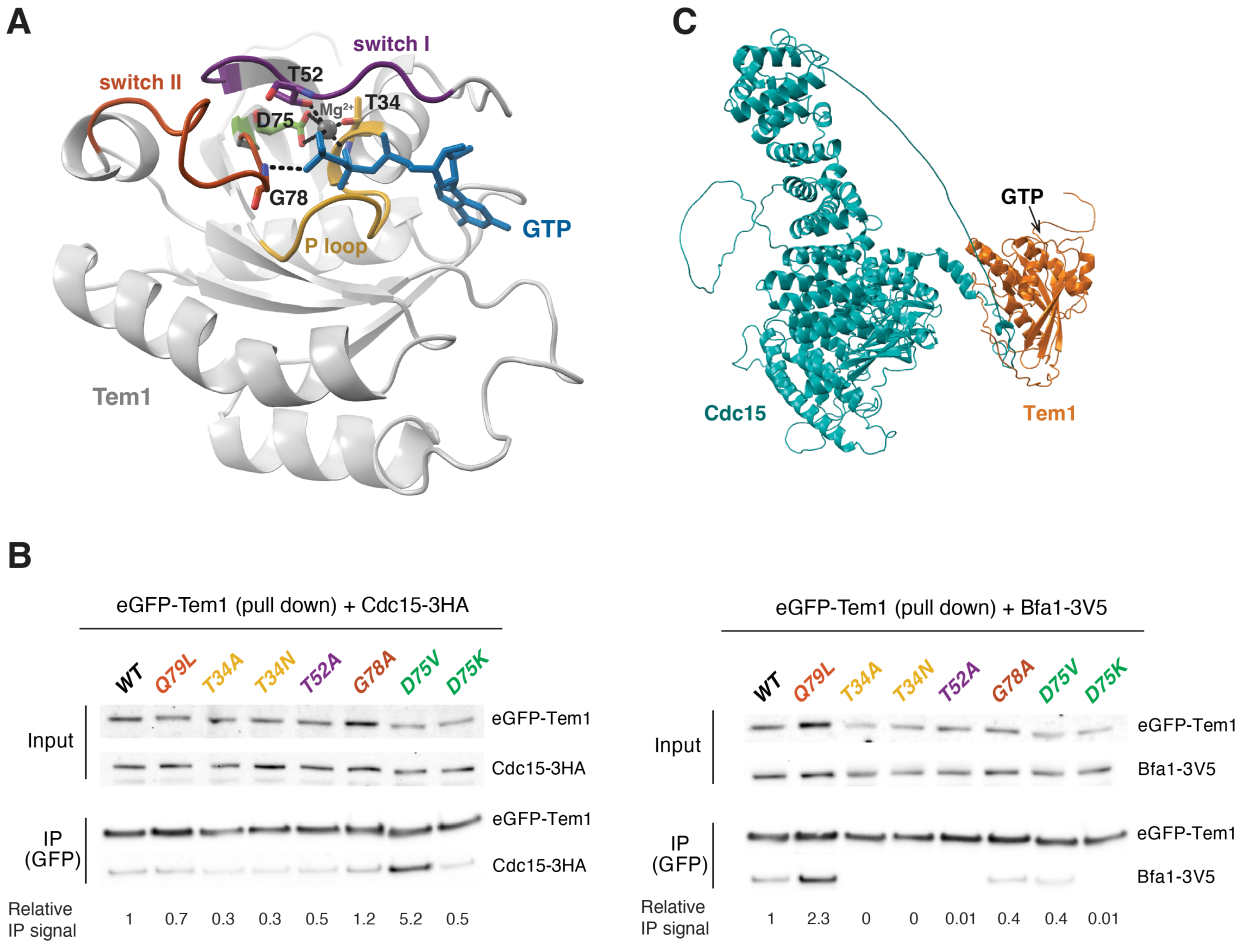

(**A**) Mutated residues in Tem1. A model of Tem1 (residues 13–187 containing the core GTPase domain) was downloaded from Swiss Model (P38987_20210204) using Rab35 (GTP)-RUSC2 as a template. Tem1 backbone (gray ribbon), GTP (cyan), Mg^{2+} (dark gray sphere), P-loop with T34 (yellow), switch-I with T52 (purple), switch-II with G78 (orange) and D75 (green). T34, T52, and D75 coordinate the Mg^{2+} atom while G78 forms hydrogen bond with the γ-phosphate (dashed lines). T34 (Ras-S17) and D75 (Ras-D57) contribute to nucleotide binding and mutations in these residues have been shown to bias affinity toward GDP over GTP for Ras. T52 (Ras-T35) and G78 (Ras-G60) are invariant residues in switch I/II regions of small GTPases that form key contacts with the γ-phosphate in GTP to stabilize the active confirmation that is used by regulatory proteins and effectors to 'sense' the nucleotide status of the small GTPases.
(**B**) Interaction between different Tem1 mutants and Cdc15 or the GAP complex via co-immunoprecipitation. yEGFP-Tem1 was immunoprecipitated from exponentially grown cells of

y2885/y2886/y3209/y3210/y3208/y3211/y3212/y3213 (Cdc15-3HA with indicated yEGFP tagged Tem1 mutants) or y3452/y3472/y3457/y3458/y3456/y3455/y3459/y3460 (Bfa1-3V5 with indicated yEGFP tagged Tem1 mutants) and the presence of Cdc15-3HA or Bfa1-3V5 were analyzed by Western blot analysis.

(**C**) AlphaFold2 predicted structure of Tem1-Cdc15 complex (DOI: 10.5452/ma-bak-cepc-0244).

Figure S3: N-terminal fusion has a minimal perturbation on Tem1.

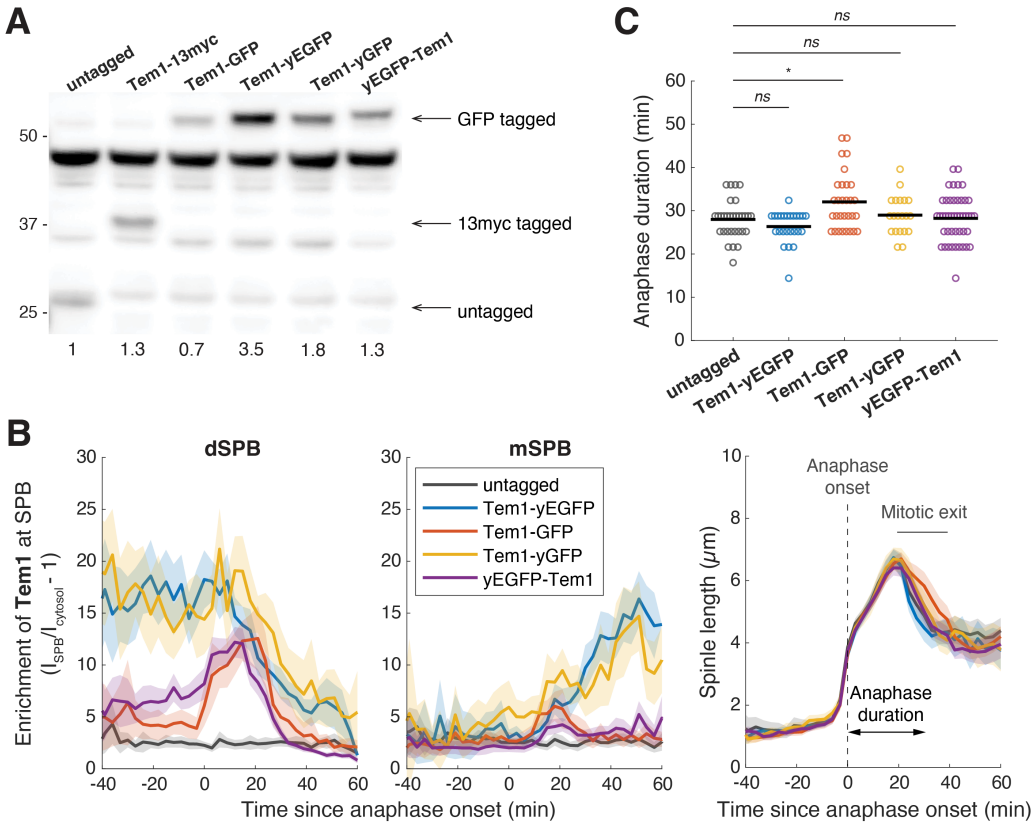

(**A**) Expression level of different Tem1 fusions. Whole-cell lysates of exponentially growing yA2587 (untagged), yA1828 (Tem1-13myc), yA22523 (Tem1-GFP), yA21089 (Tem1-yEGFP), y1724 (Tem1-yGFP), and y1735 (yEGFP-Tem1) were analyzed by western blot with serum against Tem1. Cells were grown in YPD at 30 °C. C-terminal fusions of Tem1 stabilize the protein (unless a non-codon optimized GFP fusion is used). N-terminal fusion yEGFP-Tem1 is expressed at a level similar to wild-type Tem1 (1.3x) and cells expressing this fusion exit from mitosis at a rate similar to untagged cells (C).

(**B**) SPB localization and spindle kinetics for different Tem1 fusions (y1008, y1267, y1271, y1739, and y1748; n = 39, 35, 39, 28, and 62 cells respectively) measured using the SPB marker Spc42-mScarlet-I. Cells were grown at 25 °C in SC medium + 2% glucose and imaged every 3 minutes for 4 hours. Solid lines represent the mean, shaded areas represent 95% confidence intervals. *TEM1-yEGFP* (codon-optimized eGFP) is known to be hyperactive (SPoC defective) whereas *TEM1-GFP* (not codon-optimized for yeast) is hypoactive as cells expressing Tem1-GFP delays exit from mitosis for more than 3 minutes. Tem1-yGFP (codon-optimized GFP) behaves more like Tem1-yEGFP rather than Tem1-GFP for SPB localization indicating it is the

codon usage, likely due to changes in expression level as shown in (A), that is responsible for the difference in activity and localization profiles.

(**C**) Anaphase duration of the cells shown in (B). Solid lines represent the median. *ns*, not significant ($p > 0.05$), *$p < 0.05$ by two-sided Wilcoxon rank sum test.

Figure S4: Localization of Tem1 to the SPB depends on the GAP complex Bub2-Bfa1.

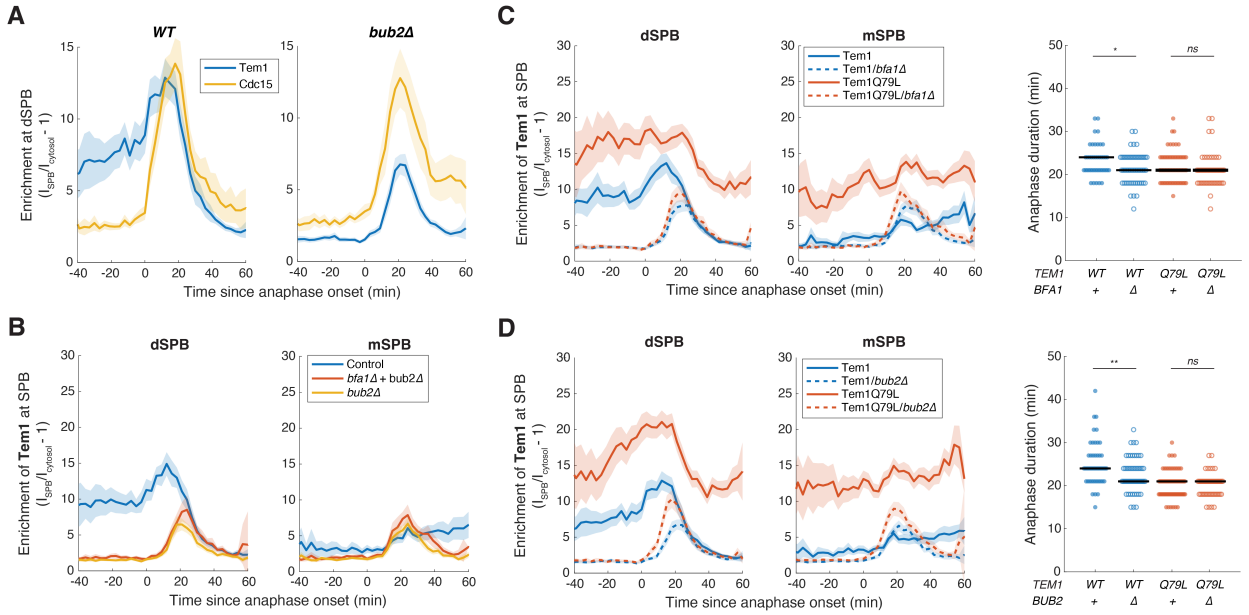

(**A**) Comparison of SPB localization for Tem1 and Cdc15 in the presence or absence of *BUB2*.

(**B**) SPB localization of Tem1 with or without *BFA1* & *BUB2*. Cells of y2015 (Tem1, $n = 44$ cells), y3717 (Tem1 in *bfa1Δ*+*bub2Δ*, $n = 42$ cells), and y3718 (Tem1 in *bub2Δ*, $n = 50$ cells) were grown at 25 °C in SC medium + 2% glucose and imaged every 3 minutes for 4 hours. Solid lines represent the average. Shaded areas represent 95% confidence intervals.

(**C-D**) SPB localization of Tem1 or the GTP-locked Tem1Q79L with or without the GAP component *BFA1* (C) or *BUB2* (D) and the anaphase duration for the corresponding cells. Cells of y2015 (Tem1, $n = 54$ cells), y2098 (Tem1 in *bfa1Δ*, $n = 64$ cells), y2019 (Tem1Q79L, $n = 79$ cells), y2133 (Tem1Q79L in *bfa1Δ*, $n = 64$ cells), and y1748 (Tem1, $n = 65$ cells), y1929 (Tem1 in *bub2Δ*, $n = 72$ cells), y1824 (Tem1Q79L, $n = 91$ cells), y1930 (Tem1Q79L in *bub2Δ*, $n = 64$ cells) were grown at 25 °C in SC medium + 2% glucose and imaged every 3 minutes for 4 hours. Solid lines represent the median. *ns*, not significant ($p > 0.05$), *$p < 0.05$ by two-sided Wilcoxon rank sum test.

Figure S5: Localization of Tem1 to the SPB depends on Cdc15.

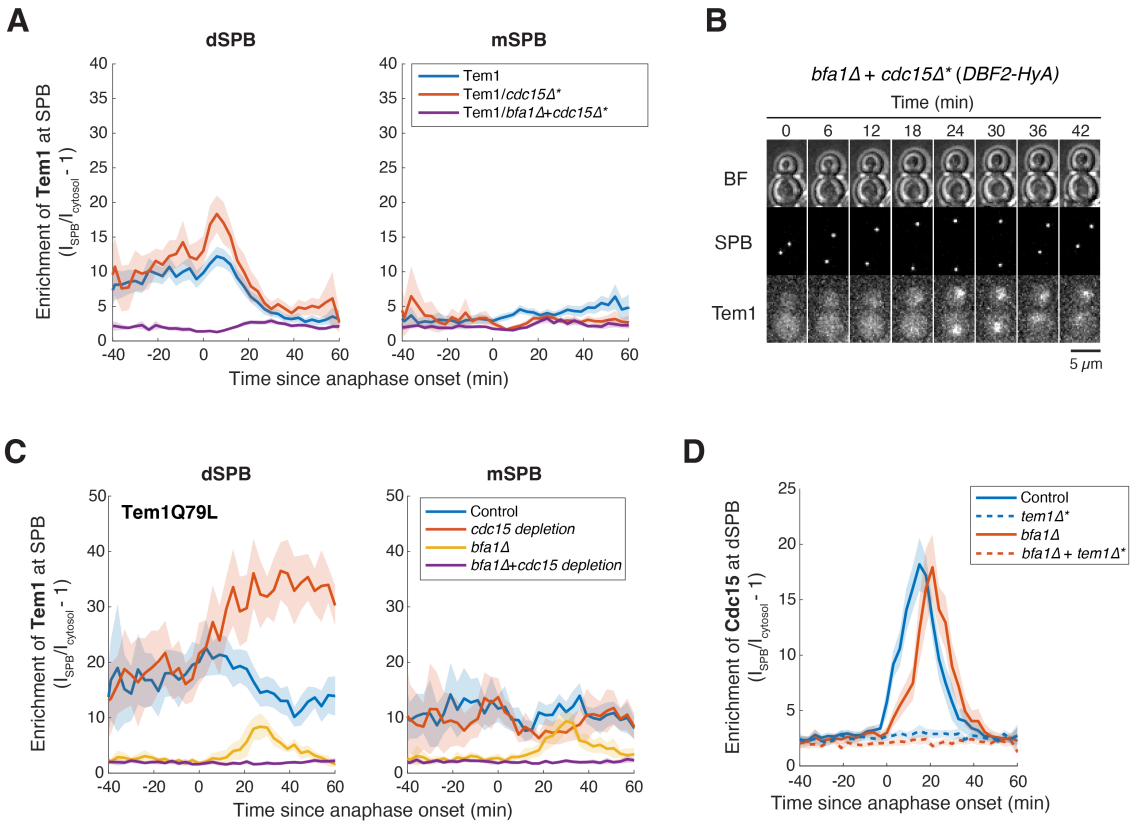

(**A**) SPB localization of Tem1 with or without *BFA1*&*CDC15*. Cells of y2898 (Tem1, *n* = 61 cells), y2910 (Tem1 in *cdc15Δ*, *n* = 24 cells), and y2899 (Tem1 in *bfa1Δ*+*cdc15Δ*, *n* = 42 cells) were grown at 25 °C in SC medium + 2% glucose and imaged every 3 minutes for 4 hours. * denotes the presence of the hyperactive *DBF2-HyA* which rescues *cdc15Δ*.

(**B**) Representative localization of Tem1 in *bfa1Δ*+*cdc15Δ* cell kept alive with *DBF2-HyA* (y2899). No SPB localization was observed but nuclear import and degradation (Fig. S12) still occurred contributing to the slight increase in SPB enrichment observed in late anaphase (A).

(**C**) SPB localization of Tem1Q79L with or without depleting Cdc15 (*CDC15-AID* +/- *osTIR*) in the presence or absence of *BFA1*. Cells of y3231 (Tem1Q79L control, *n* = 18 cells), y3226 (Tem1Q79L with Cdc15 depletion, *n* = 14 cells), y3230 (Tem1Q79L in *bfa1Δ*, *n* = 16 cells), and y3225 (Tem1Q79L in *bfa1Δ* with Cdc15 depletion, *n* = 17 cells) were grown at 25 °C in SC medium + 2% glucose + 200 μM auxin IAA and imaged every 3 minutes for 4 hours.

(**D**) SPB localization of Cdc15 still depends on Tem1 in the absence of the GAP. Cells of y1275 (Cdc15-yEGFP, *n* = 75 cells), y2945 (Cdc15-yEGFP in *tem1Δ*, *n* = 41 cells), y2958 (Cdc15-

yEGFP in *bfa1Δ*, *n* = 37 cells), and y3010 (Cdc15-yEGFP in *tem1Δ*+*bfa1Δ*, *n* = 37 cells) were grown at 25 °C in SC medium + 2% glucose and imaged every 3 minutes for 4 hours. Cells with *tem1Δ* were kept alive with *DBF2-HyA*.

Figure S6: GAP stimulated GTP hydrolysis drives the fast turnover of Tem1 at the dSPB.

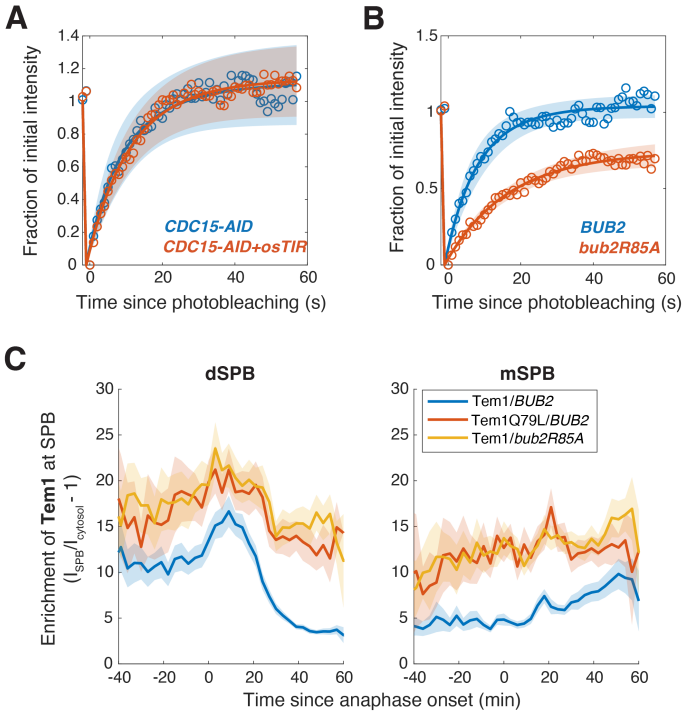

(**A**) FRAP analysis of Tem1 at dSPB in anaphase with or without depleting Cdc15. Cells of y3901 (*CDC15-AID*, *n* = 6 cells) and y3900 (*CDC15-AID+OsTIR*, *n* = 9 cells) were grown and imaged at room temperature in SC medium + 2% glucose + 100 µM IAA. Circles represent the average measurements of double normalized fluorescence intensities after correcting for photo-bleaching during acquisition. Solid lines are the average fit and shaded areas represent SD.
(**B**) FRAP analysis of Tem1 at dSPB in anaphase with hydrolysis defective Bub2 mutant (*bub2R85A*). Cells of y2015 (*BUB2*, *n* = 6 cells) and y2971 (*bub2R85A*, *n* = 6 cells) were grown and imaged at room temperature in SC medium + 2% glucose. Circles represent the average measurements of double normalized fluorescence intensities after correcting for photo-bleaching during acquisition. Solid lines are the average fit and shaded areas represent SD.
(**C**) SPB localization of Tem1 in cells with defective GTP hydrolysis. Cells of y2015 (*WT*, *n* = 69 cells), y2019 (*TEM1Q79L*, *n* = 42 cells), and y2971 (*bub2R85A*, *n* = 51 cells) were grown at 25 °C in SC medium + 2% glucose and imaged every 3 minutes for 4 hours. Solid lines represent the average. Shaded areas represent 95% confidence intervals.

Figure S7: A simple model for Tem1's nucleotide cycle.

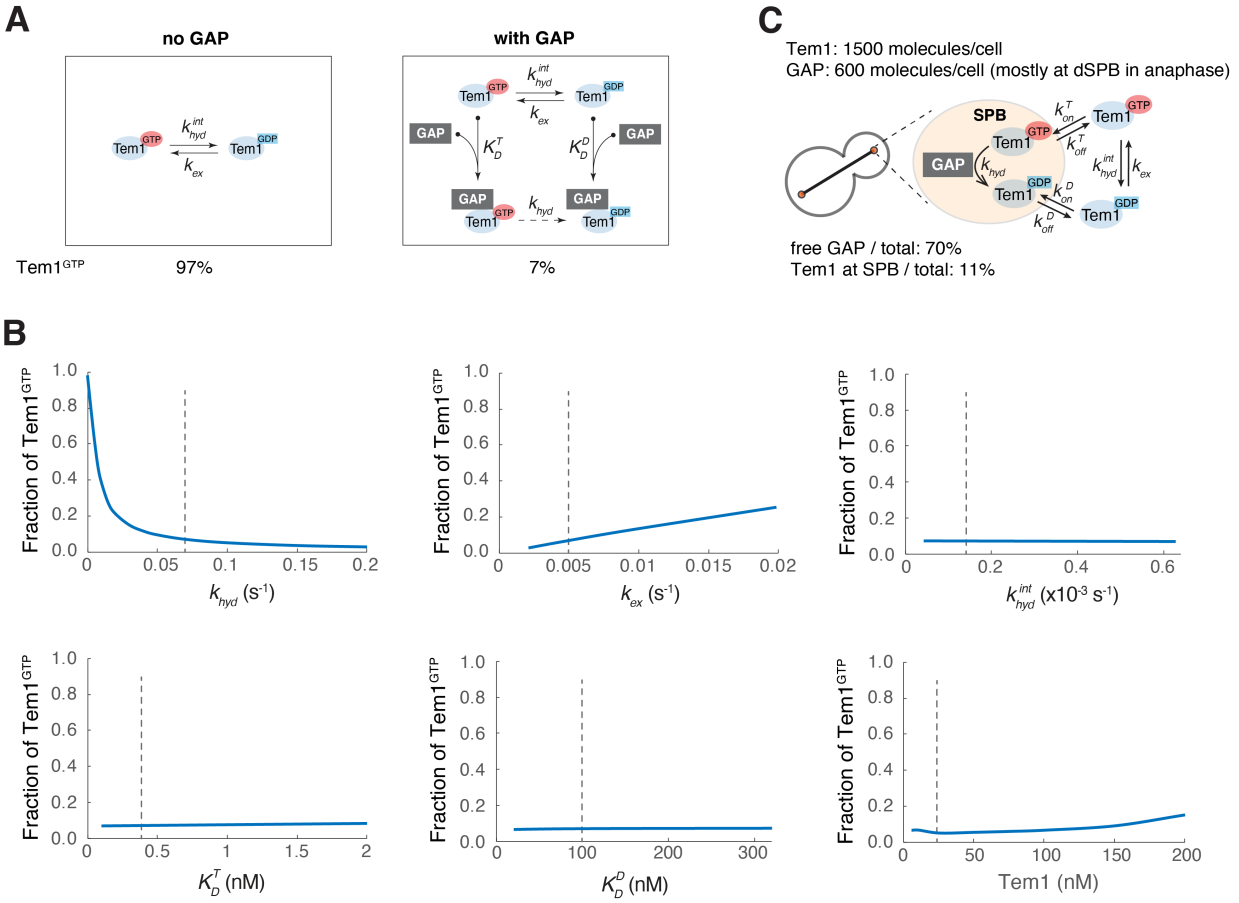

(**A**) A simplified model for Tem1's GTP/GDP cycle with or without the GAP.

(**B**) Fraction of Tem1^{GTP} as predicted by the model (with GAP) as a function of the GAP-stimulated GTP hydrolysis rate k_{hyd}, Tem1's intrinsic nucleotide exchange rate k_{ex}, Tem1's intrinsic GTP hydrolysis rate k_{hyd}^{int}, dissociation constant for GAP binding Tem1^{GTP} K_D^T, dissociation constant for GAP binding Tem1^{GDP} K_D^D, or Tem1 concentration in the cell. Dashed lines represent the values used to make the predictions shown in A.

(**C**) A simplified model for Tem1's GTP/GDP cycle at dSPB in anaphase. The same model parameters were used as in A.

Figure S8: The GAP is redistributed upon anaphase onset.

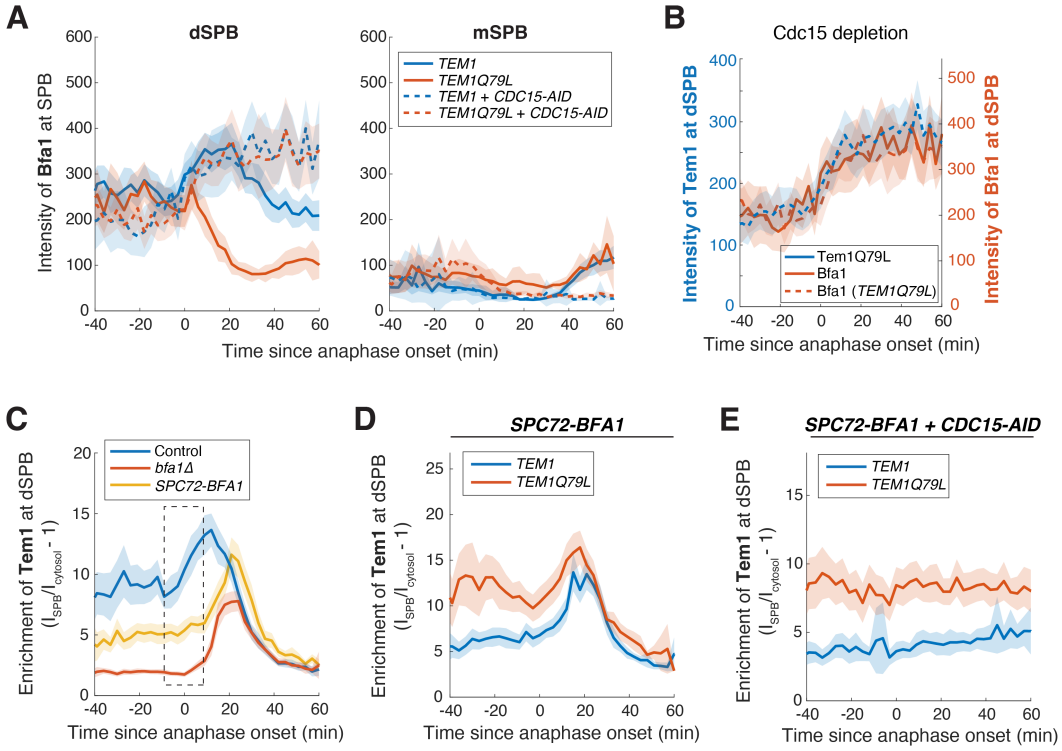

(**A**) dSPB localization of Bfa1 in cells expressing *TEM1* or *TEM1Q79L* with or without Cdc15 depleted. Cells of y1374 (*TEM1*, *n* = 42 cells), y2194 (*TEM1Q79L*, *n* = 30 cells), y4123 (*TEM1 + CDC15-AID*, *n* = 24 cells), and y4122 (*TEM1QL + CDC15-AID*, *n* = 32 cells) were grown at 25 °C in SC medium + 2% glucose + 100 µM IAA. The effect of *TEM1Q79L* on Bfa1 SPB localization depends on Cdc15. With Cdc15 depleted, Bfa1 localization to dSPB in cells expressing *TEM1Q79L* behaved the same as in cells with *TEM1*.

(**B**) Comparison of dSPB localization for Tem1Q79L (same data as in Fig. 5E), Bfa1 in *TEM1* cells (same data as in A), and Bfa1 in *TEM1Q79L* cells (same data as in A) with Cdc15 depleted.

(**C**) dSPB localization of Tem1 with or without GAP redistribution. Cells of y2015 (*BFA1*, *n* = 54 cells), y2098 (*bfa1Δ*, *n* = 64 cells), and y2990 (*SPC72-BFA1* which tethers the GAP to the SPB and prevents its redistribution, *n* = 48 cells) were grown at 25 °C in SC medium + 2% glucose. The increase in dSPB localization upon anaphase onset observed for Tem1 is driven by GAP redistribution. Tethering Bfa1 to the SPB with *SPC72-BFA1* abolished the increase upon anaphase onset (see boxed area).

(**D**) dSPB localization of Tem1 or Tem1Q79L in cells with SPB-tethered GAP (*SPC72-BFA1*). Cells of y2990 (*TEM1*, *n* = 48 cells) and y2991 (*TEM1Q79L*, *n* = 54 cells) were grown at 25 °C in SC medium + 2% glucose.

(**E**) dSPB localization of Tem1 or Tem1Q79L in cells with SPB-tethered GAP (*SPC72-BFA1*) and Cdc15 depleted (*CDC15-AID*). Cells of y3227 (*TEM1*, *n* = 53 cells) and y4106 (*TEM1Q79L*, *n* = 53 cells) were grown at 25 °C in SC medium + 2% glucose + 100 μM IAA. dSPB localization of Tem1 and Tem1Q79L remained steady when Bfa1 was tethered to the SPB in cells with Cdc15 depleted.

For all plots, cells were imaged every 3 minutes for 4 hours. Lines represent the average. Shaded areas represent 95% confidence intervals.

Figure S9: Tethering Tem1 to the SPB rescues the lethality of nucleotide binding mutants of Tem1.

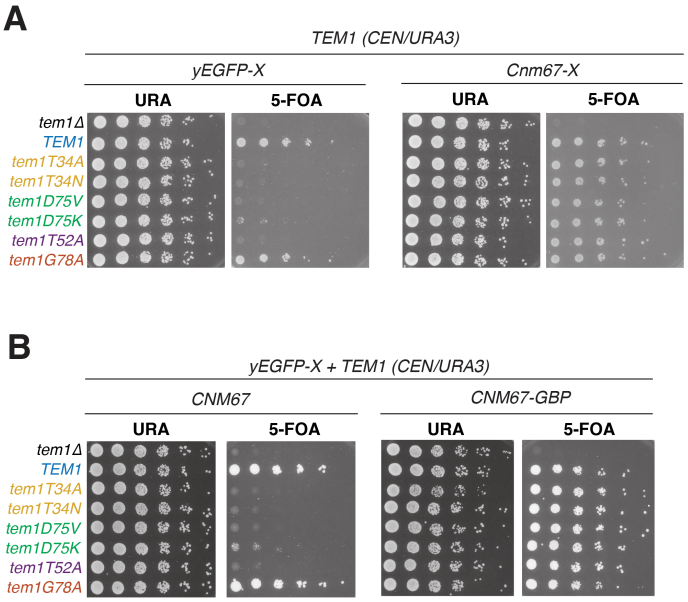

(**A**-**B**) Complementation analysis of Tem1 mutants with and without tethering to the SPB via direct fusion to Cnm67 (A) or using yGFP-Tem1 + Cnm67-GBP combo (B). 5-fold serial dilutions of strains y2891/y3202/y3203/y3204/y3206/y3207/y3214/y3205 (untethered) and y2891/y2893/y2927/y3187/y3190/y3191/y3189/y3188 (direct fusion as Cnm67-Tem1) or y3303/y3304/y3305/y3306/y3308/y3309/y3310/y3307 (with *CNM67-GBP*) were spotted onto plates with or without 5'-fluoroorotic acid (5-FOA) and incubated at 25°C for 3 to 4 days. The presence of 5-FOA selects cells that are viable after losing the *TEM1 (URA3/CEN)* plasmid. Mutations in T34, D75, and T52 render Tem1 inactive and severely reduce viability. In contrast, the switch-II effector mutant Tem1G78A is active.

Figure S10: Concentrating Tem1 by tethering to GEMs activates the MEN.

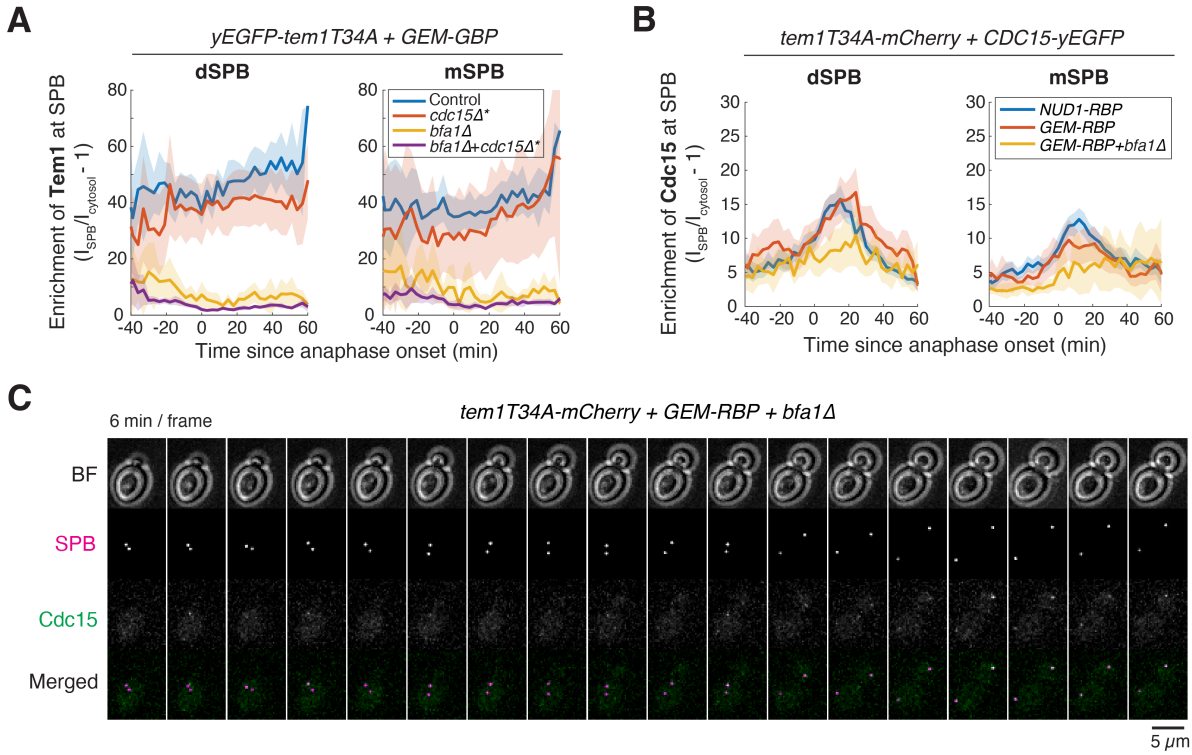

(**A**) SPB localization of GEM-tethered Tem1T34A in cells with or without *BFA1* or *CDC15*. Cells of y3630 (*BFA1*+*CDC15*, *n* = 27 cells), y3631 (*BFA1*+*cdc15Δ*, *n* = 18 cells), y3557 (*bfa1Δ*+*CDC15*, *n* = 21 cells), and y3510 (*bfa1Δ*+*cdc15Δ*, *n* = 21 cells) were grown at 25°C in SC medium + 2% glucose and imaged every 3 minutes for 4 hours. Solid lines represent the average. Shaded areas represent 95% confidence intervals.

(**B**) SPB localization of Cdc15 in cells with SPB- or GEM-tethered Tem1T34A. Cells of y3585 (*NUD1-RBP*, *n* = 67 cells), y3589 (*GEM-RBP*, *n* = 35 cells), and y3588 (GEM-RBP+*bfa1Δ*, *n* = 14 cells) were grown at 25°C in SC medium + 2% glucose and imaged every 3 minutes for 4 hours. Solid lines represent the average. Shaded areas represent 95% confidence intervals.

(**C**) Representative localization of Cdc15 in y3588.

Figure S11: MEN activity is sensitive to Tem1 level.

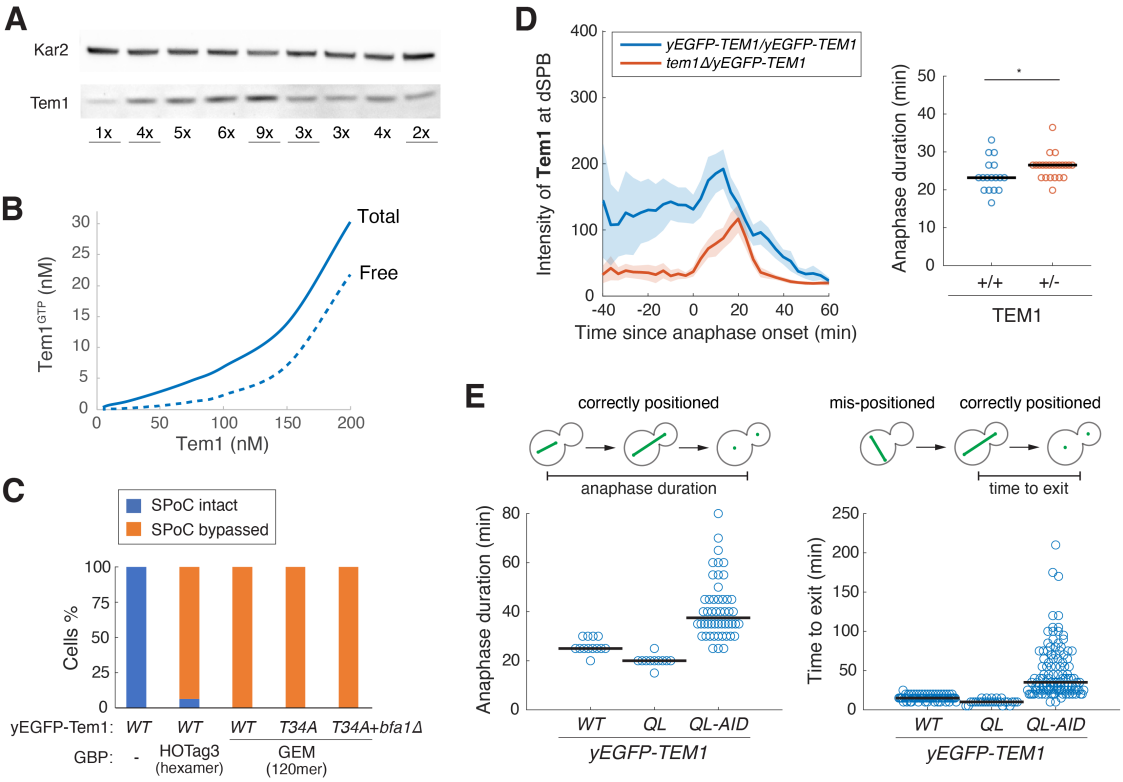

(**A**) Quantification of Tem1 expression level. Whole-cell lysates of exponentially growing cells with different copy numbers of Tem1 integrated at the *leu2* locus. Relative expression of Tem1 (indicated below) was quantified and normalized to the signal of Kar2. Underscored lanes represent strains used in this study: yA2587 (1xTem1, WT), y3693 (4xTem1), y3696 (9xTem1), y3692 (3xTem1), y3691 (2xTem1).

(**B**) Predicted $Tem1^{GTP}$ concentration as a function of Tem1 concentration in the cell (using the model illustrated in Fig. S7).

(**C**) SPoC integrity in cells with locally clustered Tem1. Cells of y4097 (yEGFP-*TEM1*, n = 31 cells), y4096 (yEGFP-*TEM1* + HOTag3-GBP, n = 63 cells), y4095 (yEGFP-*TEM1* + GEM-GBP, n = 40 cells), y4100 (yEGFP-*tem1T34A* + GEM-GBP, n = 40 cells), and y4306 (yEGFP-*tem1T34A* + GEM-GBP + *bfa1*Δ, n = 45 cells) were grown at 25 °C in SC medium + 2% glucose + 100 μM IAA to induce spindle mispositioning by depleting Dyn1 and Kar9 and imaged every 5 minutes for 5 hours. Status of the spindle and cell cycle stages were monitored with mCherry-Tub1.

(**D**) SPB localization of Tem1 (left) and distribution of anaphase duration (right) for diploid cells with two or one copy of *yEGFP-TEM1*. Cells of y3713 (two copies, n = 20 cells) and y3711 (one

copy, n = 26 cells) were grown at 25°C in SC medium + 2% glucose and imaged every 3 minutes for 4 hours. Solid lines represent the average. Shaded areas represent 95% confidence intervals. *$p < 0.05$ by two-sided Wilcoxon rank sum test. Note that the SPB localization profile of Tem1 heterozygous deletion (~50% expression level) resembles the hypomorphic Tem1-GFP (Fig. S3, ~ 70% WT level).

(**E**) Efficiency to exit from mitosis for GTP-locked Tem1 mutants with or without depletion. Same experiment as in Fig. 7E. Time to exit from mitosis as illustrated was measured for cells of y3817 (yEGFP-*TEM1*, n = 13 cells for anaphase duration and 72 cells for time to exit after correcting spindle position), y3818 (yEGFP-*TEM1Q79L*, n = 11 cells for anaphase duration and 27 cells for time to exit after correcting spindle position), and y4311 (yEGFP-*TEM1Q79L-AID**, n = 52 cells for anaphase duration and 137 cells for time to exit after correcting spindle position).

Figure S12: Tem1 level is cell cycle regulated.

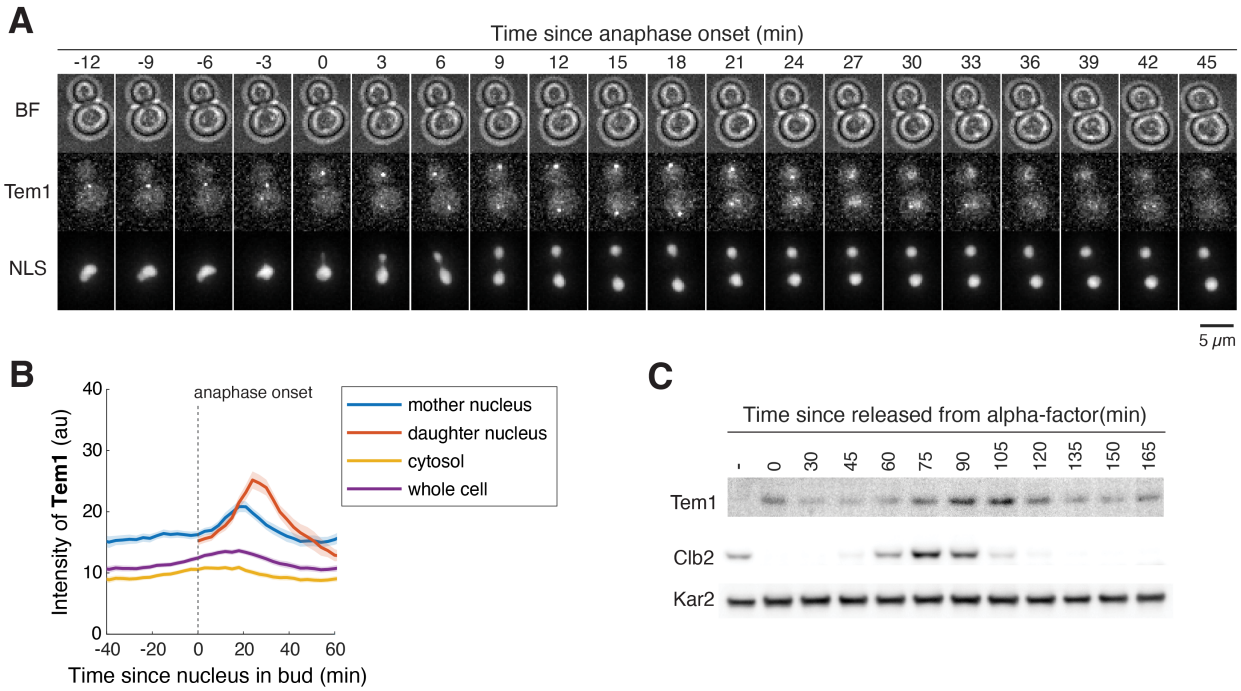

(**A**) Localization of Tem1 during the cell cycle where Tem1 is imported into the nucleus after exit from mitosis for degradation. y1879 (*yEGFP-TEM1* and *NLS$_{SV40}$-2xmCherry*) cells were grown at 25 °C in SC medium + 2% glucose and imaged every 3 minutes for 4 hours.

(**B**) Quantification of nuclear import and degradation of Tem1. Same cells as in (A). Lines represent the average; shaded areas represent 95% confidence intervals.

(**C**) Tem1 level is cell cycle regulated. yA2587 (wild-type untagged strain) was arrested in G1 with α-factor (5 μg/ml) followed by release into YPD lacking pheromone. The amount of Tem1 protein were analyzed in whole-cell lysates by Western blot with anti-Tem1 serum. Clb2 was analyzed to determine when cells were in mitosis. Kar2 was used as internal loading control.

Table S1. Yeast strains used in this study.

Strain	Relevant Genotype
A2587	*MATa, ade2-1, leu2-3, ura3, trp1-1, his3-11,15, can1-100, GAL, psi+ (wild-type W303)*
A1828	*MATa, TEM1-13Myc*
A21089	*MATa, TEM1-yEGFP::SpHIS5*
A22523	*MATa, TEM1-GFP:HisMx6*
y1008	*MATa, SPC42-mScarlet-I::LEU2*
y1267	*MATa, SPC42-mScarlet-I::LEU2, TEM1-yEGFP::SpHIS5*
y1271	*MATa, SPC42-mScarlet-I::LEU2, TEM1-GFP:HisMx6*
y1275	*MATa, SPC42-mScarlet-I::LEU2, CDC15-yEGFP::KanMX6*
y1374	*MATa, SPC42-mScarlet-I::LEU2, BFA1-yEGFP::KanMX6*
y1378	*MATa, SPC42-mScarlet-I::LEU2, BUB2-yEGFP::KanMX6*
y1584	*MATa, SPC42-mScarlet-I::LEU2, TEM1::hphNT1*
y1693	*MATa, SPC42-mScarlet-I::LEU2, CDC15-yEGFP::KanMX6, bub2::HIS3*
y1724	*MATa, TEM1-yGFP(S65T)::SpHIS5*
y1735	*MATa, yEGFP-TEM1*
y1739	*MATa, SPC42-mScarlet-I::LEU2, TEM1-yGFP(S65T)::SpHIS5*
y1748	*MATa, SPC42-mScarlet-I::LEU2, yEGFP-TEM1*
y1824	*MATa, SPC42-mScarlet-I::LEU2, yEGFP-TEM1(Q79L)*
y1879	*MATa, yEGFP-TEM1, ura3:pRS306-pCTS1-2xmCherry-SV40NLS:URA3*
y1929	*MATa, SPC42-mScarlet-I::LEU2, yEGFP-TEM1, bub2::HIS3*
y1930	*MATa, SPC42-mScarlet-I::LEU2, yEGFP-TEM1(Q79L), bub2::HIS3*
y2015	*MATa, SPC42-mScarlet-I::LEU2, yEGFP-TEM1::KanMX6*
y2019	*MATa, SPC42-mScarlet-I::LEU2, yEGFP-TEM1(Q79L)::KanMX6*
y2098	*MATa, SPC42-mScarlet-I::LEU2, yEGFP-TEM1::KanMX6, bfa1::HIS3*
y2133	*MATa, SPC42-mScarlet-I::LEU2, yEGFP-TEM1(Q79L)::KanMX6, bfa1::HIS3*
y2194	*MATa, SPC42-mScarlet-I::LEU2, BFA1-yEGFP::KanMX6, TEM1Q79L::hphNT1*
y2761	*MATa, CDC15-3HA::His3MX*
y2885	*MATa, CDC15-3HA::His3MX, yEGFP-TEM1::KanMX6*
y2886	*MATa, CDC15-3HA::His3MX, yEGFP-TEM1(Q79L)::KanMX6*
y2891	*MATa, tem1::KanMx6, pRS316-yEGFP-TEM1*
y2892	*MATalpha, tem1::KanMx6, pRS316-yEGFP-TEM1*
y2893	*MATa, pRS316-yEGFP-TEM1*
y2898	*MATa, SPC42-mScarlet-I::LEU2, yEGFP-TEM1::KanMX6, DBF2-HyA::hphNT1*
y2899	*MATa, SPC42-mScarlet-I::LEU2, yEGFP-TEM1::KanMX6, DBF2-HyA::hphNT1, bfa1::HIS3, cdc15::HIS3*
y2927	*MATa, tem1::CNM67-tem1(T34A), pRS316-yEGFP-TEM1*
y2945	*MATa, cdc15::HIS3, leu2::CDC15-yEGFP::LEU2, SPC42-mScarlet-I::LEU2, pRS315-DBF2-HyA, tem1::KanMx6*
y2958	*MATa, SPC42-mScarlet-I::LEU2, CDC15-yEGFP::KanMX6, bfa1::HIS3*
y2971	*MATa, SPC42-mScarlet-I::LEU2, yEGFP-TEM1::KanMX6, bub2(R85A)*
y2990	*MATalpha, SPC42-mScarlet-I::LEU2, yEGFP-TEM1::KanMX6, SPC72-BFA1::LEU2, bfa1::TRP1*
y2991	*MATa, SPC42-mScarlet-I::LEU2, yEGFP-TEM1(Q79L)::KanMX6, SPC72-BFA1::LEU2, bfa1::TRP1*

y3010	*MATa, SPC42-mScarlet-I::LEU2, CDC15-yEGFP::KanMX6, pRS315-DBF2-HyA, tem1::KanMx6, bfa1::HIS3*
y3059	*MATa, yEGFP-Tem1::KanMX6, dbf2::DBF2-HyA::hphNT1*
y3099	*MATa, SPC42-mScarlet-I::LEU2, BFA1-yEGFP::KanMX6, bub2::HIS3*
y3147	*MATa, SPC42-mScarlet-I::LEU2, yEGFP-tem1(T52A)::KanMX6, DBF2-HyA::hphNT1*
y3167	*MATa, SPC42-mScarlet-I::LEU2, yEGFP-tem1(T34A)::KanMX6, DBF2-HyA::hphNT1*
y3171	*MATalpha, SPC42-mScarlet-I::LEU2, yEGFP-tem1(T34N)::KanMX6, DBF2-HyA::hphNT1*
y3187	*MATa, tem1::CNM67-tem1(T34N), pRS316-yEGFP-TEM1*
y3188	*MATa, tem1::CNM67-TEM1(G78A), pRS316-yEGFP-TEM1*
y3189	*MATa, tem1::CNM67-tem1(T52A), pRS316-yEGFP-TEM1*
y3190	*MATa, tem1::CNM67-tem1(D75V), pRS316-yEGFP-TEM1*
y3191	*MATa, tem1::CNM67-tem1(D75K), pRS316-yEGFP-TEM1*
y3202	*MATa, yEGFP-TEM1::KanMX6, pRS316-yEGFP-TEM1*
y3203	*MATa, yEGFP-tem1(T34A)::KanMX6, pRS316-yEGFP-TEM1*
y3204	*MATa, yEGFP-tem1(T34N)::KanMX6, pRS316-yEGFP-TEM1*
y3205	*MATa, yEGFP-TEM1(G78A)::KanMX6, pRS316-yEGFP-TEM1*
y3206	*MATa, yEGFP-tem1(D75V)::KanMX6, pRS316-yEGFP-TEM1*
y3207	*MATa, yEGFP-tem1(D75K)::KanMX6, pRS316-yEGFP-TEM1*
y3208	*MATa, CDC15-3HA::His3MX, yEGFP-tem1(T52A)::KanMX6, DBF2-HyA::hphNT1*
y3209	*MATa, CDC15-3HA::His3MX, yEGFP-tem1(T34A)::KanMX6, DBF2-HyA::hphNT1*
y3210	*MATa, CDC15-3HA::His3MX, yEGFP-tem1(T34N)::KanMX6, DBF2-HyA::hphNT1*
y3211	*MATa, CDC15-3HA::His3MX, yEGFP-TEM1(G78A)::KanMX6, DBF2-HyA::hphNT1*
y3212	*MATa, CDC15-3HA::His3MX, yEGFP-tem1(D75V)::KanMX6, DBF2-HyA::hphNT1*
y3213	*MATa, CDC15-3HA::His3MX, yEGFP-tem1(D75K)::KanMX6, DBF2-HyA::hphNT1*
y3214	*MATa, yEGFP-tem1(T52A)::KanMX6, pRS316-yEGFP-TEM1*
y3223	*MATalpha, SPC42-mScarlet-I::LEU2, yEGFP-TEM1::KanMX6, bfa1::HIS3, CDC15-AID*-9myc::hphNT1, leu2::pTEF1-osTIR::LEU2*
y3224	*MATalpha, SPC42-mScarlet-I::LEU2, yEGFP-TEM1::KanMX6, CDC15-AID*-9myc::hphNT1, leu2::pTEF1-osTIR::LEU2*
y3225	*MATa, SPC42-mScarlet-I::LEU2, yEGFP-TEM1(Q79L)::KanMX6, bfa1::HIS3, CDC15-AID*-9myc::hphNT1, leu2::pTEF1-osTIR::LEU2*
y3226	*MATalpha, SPC42-mScarlet-I::LEU2, yEGFP-TEM1(Q79L)::KanMX6, CDC15-AID*-9myc::hphNT1, leu2::pTEF1-osTIR::LEU2*
y3227	*MATa, SPC42-mScarlet-I::LEU2, yEGFP-TEM1::KanMX6, SPC72-BFA1::LEU2, bfa1::TRP1, CDC15-AID*-9myc::HYG, his3::pTEF1-osTIR::HIS3*
y3228	*MATa, SPC42-mScarlet-I::LEU2, yEGFP-TEM1::KanMX6, bfa1::HIS3, CDC15-AID*-9myc::hphNT1*
y3229	*MATa, SPC42-mScarlet-I::LEU2, yEGFP-TEM1::KanMX6, CDC15-AID*-9myc::hphNT1*
y3230	*MATa, SPC42-mScarlet-I::LEU2, yEGFP-TEM1(Q79L)::KanMX6, bfa1::HIS3, CDC15-AID*-9myc::hphNT1*
y3231	*MATa, SPC42-mScarlet-I::LEU2, yEGFP-TEM1(Q79L)::KanMX6, CDC15-AID*-9myc::hphNT1*
y3287	*MATa, yEGFP-TEM1(Q79L)::KanMX6, CNM67-GBP::His3MX6*
y3289	*MATa, yEGFP-TEM1::KanMX6, CNM67-GBP::His3MX6*
y3291	*MATa, yEGFP-tem1(T34A)::KanMX6, CNM67-GBP::His3MX6*
y3303	*MATa, tem1::KanMx6, pRS316-yEGFP-TEM1, CNM67-GBP::His3MX6*

y3304	*MATa, yEGFP-TEM1::KanMX6, pRS316-yEGFP-TEM1, CNM67-GBP::His3MX6*
y3305	*MATa, yEGFP-tem1(T34A)::KanMX6, pRS316-yEGFP-TEM1, CNM67-GBP::His3MX6*
y3306	*MATa, yEGFP-tem1(T34N)::KanMX6, pRS316-yEGFP-TEM1, CNM67-GBP::His3MX6*
y3307	*MATa, yEGFP-TEM1(G78A)::KanMX6, pRS316-yEGFP-TEM1, CNM67-GBP::His3MX6*
y3308	*MATa, yEGFP-tem1(D75V)::KanMX6, pRS316-yEGFP-TEM1, CNM67-GBP::His3MX6*
y3309	*MATa, yEGFP-tem1(D75K)::KanMX6, pRS316-yEGFP-TEM1, CNM67-GBP::His3MX6*
y3310	*MATa, yEGFP-tem1(T52A)::KanMX6, pRS316-yEGFP-TEM1, CNM67-GBP::His3MX6*
y3452	*MATa, yEGFP-TEM1::KanMX6, BFA1-3V5::HIS3*
y3455	*MATa, yEGFP-TEM1(G78A)::KanMX6, BFA1-3V5::HIS3*
y3456	*MATa, yEGFP-tem1(T52A)::KanMX6, DBF2-HyA::hphNT1, BFA1-3V5::HIS3*
y3457	*MATa, yEGFP-tem1(T34A)::KanMX6, DBF2-HyA::hphNT1, BFA1-3V5::HIS3*
y3458	*MATa, yEGFP-tem1(T34N)::KanMX6, DBF2-HyA::hphNT1, BFA1-3V5::HIS3*
y3459	*MATa, yEGFP-tem1(D75V)::KanMX6, DBF2-HyA::hphNT1, BFA1-3V5::HIS3*
y3460	*MATa, yEGFP-tem1(D75K)::KanMX6, DBF2-HyA::hphNT1, BFA1-3V5::HIS3*
y3461	*MATa, BFA1-3V5::HIS3*
y3472	*MATa, yEGFP-TEM1(Q79L)::KanMX6, BFA1-3V5::HIS3*
y3499	*MATa, yEGFP-tem1(T34A)::KanMX6, pRS316-yEGFP-TEM1, SPC72-GBP::His3MX6*
y3500	*MATa, yEGFP-tem1(T34A)::KanMX6, pRS316-yEGFP-TEM1, NUD1-GBP::His3MX6*
y3502	*MATa, yEGFP-tem1(T34A)::KanMX6, pRS316-yEGFP-TEM1, leu2::pRS305-pINO4-PfV-GS-GBP::LEU2*
y3510	*MATa, yEGFP-tem1(T34A)::KanMX6, leu2::pRS305-pINO4-PfV-GS-GBP::LEU2, cdc15::HIS3, DBF2-HyA::hphNT1, SPC42-mScarlet-I::LEU2, bfa1::TRP1*
y3557	*MATa, yEGFP-tem1(T34A)::KanMX6, leu2::pRS305-pINO4-PfV-GS-GBP::LEU2, SPC42-mScarlet-I::LEU2, bfa1::TRP1*
y3585	*MATa, SPC42-mScarlet-I::LEU2, CDC15-yEGFP::KanMX6, tem1T34A-mCherry-PIF6::NatMx6, NUD1-RBP::His3MX6*
y3588	*MATa, SPC42-mScarlet-I::LEU2, CDC15-yEGFP::KanMX6, tem1T34A-mCherry-PIF6::NatMx6, leu2::pRS305-pINO4-PfV-GS-RBP::LEU2, bfa1::HIS3*
y3589	*MATa, SPC42-mScarlet-I::LEU2, CDC15-yEGFP::KanMX6, tem1T34A-mCherry-PIF6::NatMx6, leu2::pRS305-pINO4-PfV-GS-RBP::LEU2*
y3630	*MATa, yEGFP-tem1(T34A)::KanMX6, leu2::pRS305-pINO4-PfV-GS-GBP::LEU2, SPC42-mScarlet-I::LEU2*
y3631	*MATa, yEGFP-tem1(T34A)::KanMX6, leu2::pRS305-pINO4-PfV-GS-GBP::LEU2, cdc15::HIS3, DBF2-HyA::hphNT1, SPC42-mScarlet-I::LEU2*
y3632	*MATa, SPC42-mScarlet-I::LEU2, BUB2-yEGFP::KanMX6, bfa1::HIS3*
y3691	*MATa, leu2:: YIplac128-TEM1::LEU2*
y3692	*MATa, leu2::2xYIplac128-TEM1::LEU2*
y3693	*MATa, leu2::3xYIplac128-TEM1::LEU2*
y3696	*MATa, leu2::8xYIplac128-TEM1::LEU2*
y3711	*MATa/alpha, SPC42-mScarlet-I::LEU2/SPC42-mScarlet-I::LEU2, tem1::KanMx/yEGFP-TEM1::KanMx6*
y3713	*MATa/alpha, SPC42-mScarlet-I::LEU2/SPC42-mScarlet-I::LEU2, yEGFP-TEM1::KanMx/yEGFP-TEM1::KanMx6*
y3717	*MATa, SPC42-mScarlet-I::LEU2, yEGFP-TEM1::KanMX6, bub2::HIS3, bfa1::TRP1*
y3718	*MATa, SPC42-mScarlet-I::LEU2, yEGFP-TEM1::KanMX6, bub2::HIS3*
y3729	*MATa, DYN1-3V5-AID:KanMX6, KAR9-AID*-6HA:hphNT1, ura3::pTUB1-GFP-TUB1::URA3, his3::pTEF1-osTIR::HIS3, leu2::YIplac128-TEM1::LEU2*

y3730	*MATa, DYN1-3V5-AID:KanMX6, KAR9-AID*-6HA:hphNT1, ura3::pTUB1-GFP-TUB1::URA3, his3::pTEF1-osTIR::HIS3, leu2::3xYIplac128-TEM1::LEU2*
y3732	*MATa, DYN1-3V5-AID:KanMX6, KAR9-AID*-6HA:hphNT1, ura3::pTUB1-GFP-TUB1::URA3, his3::pTEF1-osTIR::HIS3, leu2::8xYIplac128-TEM1::LEU2*
y3733	*MATa, DYN1-3V5-AID:KanMX6, KAR9-AID*-6HA:hphNT1, ura3::pTUB1-GFP-TUB1::URA3, his3::pTEF1-osTIR::HIS3*
y3815	*MATa, DYN1-3V5-AID:KanMX6, KAR9-AID*-6HA:hphNT1, ura3::pTUB1-GFP-TUB1::URA3, his3::pTEF1-osTIR::HIS3, bfa1::TRP1*
y3816	*MATa, DYN1-3V5-AID:KanMX6, KAR9-AID*-6HA:hphNT1, ura3::pTUB1-GFP-TUB1::URA3, his3::pTEF1-osTIR::HIS3, leu2::2xYIplac128-TEM1::LEU2*
y3817	*MATa, yEGFP-TEM1::KanMX6, Dyn1-3V5-AID:KanMX, KAR9-AID*-6HA:hphMX, ura3:: pTUB1-GFP-TUB1::URA3, his3::pTEF1-osTIR::HIS3*
y3818	*MATa, yEGFP-TEM1(Q79L)::KanMX6, Dyn1-3V5-AID:KanMX, KAR9-AID*-6HA:hphMX, ura3:: pTUB1-GFP-TUB1::URA3, his3::pTEF1-osTIR::HIS3*
y3900	*MATa, SPC42-mScarlet-I::LEU2, yEGFP-TEM1::KanMX6, CDC15-AID*-9myc::HYG, his3::pTEF1-osTIR::HIS3*
y3901	*MATa, SPC42-mScarlet-I::LEU2, yEGFP-TEM1::KanMX6, CDC15-AID*-9myc::HYG*
y3903	*MATa, SPC42-mScarlet-I::LEU2, yEGFP-TEM1(Q79L)::KanMX6, CDC15-AID*-9myc::HYG, his3::pTEF1-osTIR::HIS3*
y3945	*MATa, yEGFP-tem1(T34A)::KanMX6, pRS316-yEGFP-TEM1, leu2::pRS305-pINO4-PfV-GS-GBP::LEU2, bfa1::TRP1*
y3948	*MATa, yEGFP-tem1(T34A)::KanMX6, pRS316-yEGFP-TEM1, bfa1::TRP1*
y3956	*MATa, yEGFP-tem1(T34A)::KanMX6, pRS316-yEGFP-TEM1, leu2::pRS305-pINO4-HOTag3-GS-GBP::LEU2*
y3958	*MATa, yEGFP-tem1(T34A)::KanMX6, pRS316-yEGFP-TEM1, leu2::pRS305-pINO4-HOTag6-GS-GBP::LEU2*
y3970	*MATa, tem1::KanMX6, pRS316-yEGFP-TEM1, leu2::pRS305-pINO4-PfV-GS-GBP::LEU2*
y3971	*MATa, tem1::KanMX6, pRS316-yEGFP-TEM1, bfa1::TRP1*
y3972	*MATa, tem1::KanMX6, pRS316-yEGFP-TEM1, leu2::pRS305-pINO4-PfV-GS-GBP::LEU2, bfa1::TRP1*
y3973	*MATa, yEGFP-TEM1::KanMX6, pRS316-yEGFP-TEM1, leu2::pRS305-pINO4-PfV-GS-GBP::LEU2*
y3974	*MATa, yEGFP-TEM1::KanMX6, pRS316-yEGFP-TEM1, bfa1::TRP1*
y3975	*MATa, yEGFP-TEM1::KanMX6, pRS316-yEGFP-TEM1, leu2::pRS305-pINO4-PfV-GS-GBP::LEU2, bfa1::TRP1*
y3976	*MATa, yEGFP-tem1(T34N)::KanMX6, pRS316-yEGFP-TEM1, leu2::pRS305-pINO4-PfV-GS-GBP::LEU2*
y3977	*MATa, yEGFP-tem1(T34N)::KanMX6, pRS316-yEGFP-TEM1, bfa1::TRP1*
y3978	*MATalpha, yEGFP-tem1(T34N)::KanMX6, pRS316-yEGFP-TEM1, leu2::pRS305-pINO4-PfV-GS-GBP::LEU2, bfa1::TRP1*
y3985	*MATa, yEGFP-tem1(T52A)::KanMX6, pRS316-yEGFP-TEM1, leu2::pRS305-pINO4-PfV-GS-GBP::LEU2*
y3986	*MATa, yEGFP-tem1(T52A)::KanMX6, pRS316-yEGFP-TEM1, bfa1::TRP1*
y3987	*MATa, yEGFP-tem1(T52A)::KanMX6, pRS316-yEGFP-TEM1, leu2::pRS305-pINO4-PfV-GS-GBP::LEU2, bfa1::TRP1*
y4095	*MATa, DYN1-3V5-AID:KanMX6, KAR9-AID*-6HA:hphNT1, his3::pTEF1-osTIR::HIS3, ura3::pTUB1-mCherry-TUB1::URA3, yEGFP-TEM1::KanMX6, leu2::pRS305-pINO4-PfV-GS-GBP::LEU2*

y4096	*MATa, DYN1-3V5-AID:KanMX6, KAR9-AID*-6HA:hphNT1, his3::pTEF1-osTIR::HIS3, ura3::pTUB1-mCherry-TUB1::URA3, yEGFP-TEM1::KanMX6, leu2::pRS305-pINO4-HOTag3-GS-GBP::LEU2*
y4097	*MATa, DYN1-3V5-AID:KanMX6, KAR9-AID*-6HA:hphNT1, his3::pTEF1-osTIR::HIS3, ura3::pTUB1-mCherry-TUB1::URA3, yEGFP-TEM1::KanMX6*
y4100	*MATa, DYN1-3V5-AID:KanMX6, KAR9-AID*-6HA:hphNT1, his3::pTEF1-osTIR::HIS3, ura3::pTUB1-mCherry-TUB1::URA3, yEGFP-tem1(T34A)::KanMX6, leu2::pRS305-pINO4-PfV-GS-GBP::LEU2*
y4106	*MATa, SPC42-mScarlet-I::LEU2, yEGFP-TEM1(Q79L)::KanMX6, SPC72-BFA1::LEU2, bfa1::TRP1, CDC15-AID*-9myc::HYG, his3::pTEF1-osTIR::HIS3*
y4122	*MATa, SPC42-mScarlet-I::LEU2, BFA1-yEGFP::KanMX6, TEM1(Q79L)::hphNT1, CDC15-AID*-9myc::HYG, his3::pTEF1-osTIR::HIS3*
y4123	*MATa, SPC42-mScarlet-I::LEU2, BFA1-yEGFP::KanMX6, CDC15-AID*-9myc::HYG, his3::pTEF1-osTIR::HIS3*
y4306	*MATa, DYN1-3V5-AID:KanMX6, KAR9-AID*-6HA:hphNT1, his3::pTEF1-osTIR::HIS3, ura3::pTUB1-mCherry-TUB1::URA3, yEGFP-tem1(T34A)::KanMX6, leu2::pRS305-pINO4-PfV-GS-GBP::LEU2, bfa1::TRP1*
y4311	*MATa, yEGFP-TEM1(Q79L)-AID*-9myc::hphMX, Dyn1-3V5-AID:KanMX, KAR9-AID*-6HA:hphMX, ura3:: pTUB1-GFP-TUB1::URA3, his3::pTEF1-osTIR::HIS3*

Table S2. Plasmids used in this study.

Plasmid	Description	Source
p998	pFA6a-link-yEGFP-SpHIS5	EUROSCARF
p1804	pRS316-eGFP-Tem1	This study
p2579	pCOLADuet-1_14xHIS-SUMO-Tem1	This study
p2717	YIplac128-Tem1 (pSP596)	S. Piatti
p2718	YIplac128-Tem1-Q79L (pSP597)	S. Piatti
p2816	pFA6a-hphN-Dbf2-HyA	This study
p2868	pFA6a-Vinnylinker-mScarlet-I-cgLEU2 (pUB1571)	E. Unal
p2888	pFA6a-hphN-Tem1Q79L	This study
p2911	pPGK1-Cas9-LEU (bRA90)	J. Haber
p2930	pFA6a-linker-yGFP(S65T)-SpHIS5	This study
p2938	pRS305-pINO4-PfV-GS-Sapphire (pLH497)	L. Holt
p3009	pFA6a-link-GBP-SpHIS5	This study
p3010	pFA6a-link-RBP-SpHIS5	This study
p3011	pRS305-pINO4-PfV-GS-GBP	This study
p3013	pRS305-pINO4-PfV-GS-RBP	This study
p3021	pCOLADuet-1-14xHIS-SUMO-Tem1Q79L	This study
p3034	pDW363_AviTag-His6-Tem1_BirA	This study
p3045	pRS305-pINO4-HOTag3-GS-GBP	This study
p3046	pRS305-pINO4-HOTag6-GS-GBP	This study